NASA MEMO 10-2-58A

NASA

MEMORANDUM

Class. Changed to Unclassified

RE-ENTRY AND RECOVERY OF NEAR-EARTH SATELLITES, WITH PARTICULAR ATTENTION TO A MANNED VEHICLE

By Alfred J. Eggers, Jr., and Thomas J. Wong

Ames Research Center
Moffett Field, Calif.

NATIONAL AERONAUTICS AND SPACE ADMINISTRATION

WASHINGTON

October 1958

NATIONAL AERONAUTICS AND SPACE ADMINISTRATION

NASA MEMO 10-2-58A

RE-ENTRY AND RECOVERY OF NEAR-EARTH SATELLITES, WITH PARTICULAR ATTENTION TO A MANNED VEHICLE*

By Alfred J. Eggers, Jr., and Thomas J. Wong

SUMMARY

General features of the motion and heating of satellites entering the atmosphere from more or less circular orbits near the earth are discussed. Attention is focused on the re-entry and recovery of manned vehicles, and it is indicated that a lifting configuration is attractive for this application because of its reduced decelerations and increased maneuverability. If the configuration develops both high lift and high drag, it is also indicated that aerodynamic heating problems remain well within tractable limits. The lower half of a body of revolution of low fineness ratio exhibits these characteristics as well as inherent stability. The paper concludes with a discussion of the key results of a theoretical and experimental investigation of a vehicle of this type which appears well suited for manned re-entry and recovery.

INTRODUCTION

Successful re-entry and recovery are desirable features of earth satellites which accumulate information, and they are essential features of manned satellites. The problems of re-entry are numerous, but primarily they evolve from the tendency of a vehicle to experience excessive aerodynamic heating and excessive aerodynamic forces with resultant high decelerations. The problem of recovery or landing is less severe, although certainly deserving of careful attention to insure that its solution does not aggravate the re-entry problem.

The concern of this paper will be primarily with manned vehicles in which the pilot plays an active role during re-entry as well as orbiting flight. Accordingly, configurations of greatest interest to us may be compromises in the sense that they have acceptably low heating and decelerations, but not necessarily minimum values of either. By the same token

*Title, Unclassified

we will not insist on configurations with a highly sophisticated landing capability. Indeed we will find it acceptable if they are susceptible to simple, reliable recovery by parachute.

With these thoughts in mind it will be helpful to commence the study with some general considerations of motion and heating during re-entry. The techniques of analysis which will prove well suited for this purpose are those of references 1 and 2, generalized and applied in a manner which has previously been given only limited distribution. The reader will be aware, of course, that a number of other studies of satellite re-entry are now available in the literature, including those of Kemp and Riddel (ref. 3), and Ferri (ref. 4), while for various planetary atmospheres there is the work of Gazley (ref. 5) and, more recently and extensively, of Chapman (ref. 6).

Following the general considerations of motion and heating we will take up the question of manned vehicles and one such vehicle which is suggested by these considerations will be considered in some detail. The characteristics of this vehicle at subsonic and low supersonic speeds were investigated by Bruce E. Tinling, while the re-entry trajectory and heating were analyzed by John O. Reller, Jr. Structural factors were considered by Charles A. Hermach, and flying qualities were studied by George A. Rathert, Jr.

MOTION AND HEATING DURING RE-ENTRY

Re-entry trajectories which are initially only slightly inclined to the horizontal are characterized by reduced decelerations and heating rates (see refs. 1 and 7), so we will consider the trajectories of this type shown in figure 1. These are, in particular, the ballistic, glide, and skip trajectories. It is noted that the range covered during re-entry tends to be smallest for the ballistic vehicle while that for the skip and glide vehicles tends to be larger depending upon the lift-drag ratio (ref. 2). However, the subsequent considerations will be based on the assumption that range during re-entry is of secondary importance, while low heating and deceleration are of primary importance. There are, of course, exceptional cases where this assumption does not apply; however, it is in general true and it substantially simplifies the consideration of the re-entry problem.

It is evident from figure 1 that the skip trajectory has the steepest entry angle of the three shown. As suggested earlier, and discussed in some detail in references 2 and 8, the skip vehicle in this event experiences more severe accelerations than a comparable glide vehicle. In addition, the skip vehicle poses more severe aerodynamic heating problems than either glide or ballistic vehicles (see refs. 2 and 8). For these reasons and since range during re-entry is considered to be of secondary

importance, we view the skip trajectory as being the least attractive of the three cited. This trajectory will not, therefore, be considered further herein.

Analysis of Ballistic and Gliding Re-entry

Motion.- In the analysis of ballistic and gliding motion we will employ the notation shown in figure 2 (see also appendix A) and assume a nonrotating earth and atmosphere. Aerodynamic lift L and drag D act as shown at the altitude y, and the inclination of the flight path and flight velocity V to the local horizontal is θ. The local radius of curvature of the flight path is r_c, and the gravity force on the vehicle is mg acting toward the center of the earth of radius r_o. Thus the parametric equations of motion normal and parallel to the flight path are, respectively,

$$\left.\begin{aligned} L + \frac{mV^2}{r_c} &= mg\left(\frac{r_o}{r}\right)^2 \cos\theta \\ D + m\frac{dV}{dt} &= -mg\left(\frac{r_o}{r}\right)^2 \sin\theta \end{aligned}\right\} \tag{1}$$

With the assumptions that $|\theta| \ll 1$, $|mg\theta| \ll D$ and $y/r_o \ll 1$, and that the exponential altitude-density relationship $\rho/\rho_o = \alpha e^{-\beta y}$ holds in the re-entry phase of flight, we can combine these equations into the following single equation for the case of constant C_D and L/D[1]

$$\frac{d^2f}{dZ^2} + \frac{I}{f}\left(1 - e^{-Z}\right) + J = 0 \tag{2}$$

where

---

[1]These parametric equations of motion can also be combined into a single equation in the altitude-range coordinate system, namely,

$$\frac{m}{C_D\alpha\rho_o A} e^{\beta y}\frac{d^3y}{ds^3} = \frac{1}{r_o} - \frac{d^2y}{ds^2} + \frac{C_L\alpha\rho_o A e^{-\beta y}}{2m} - \frac{\beta}{2}\frac{L}{D}\frac{dy}{ds}$$

however, this expression is substantially less tractable for our purpose than equation (2).

$$
\left.
\begin{aligned}
f &= e^{-\beta y} \\
Z &= \ln\left(\frac{V}{V_E}\right)^2 \\
I &= \frac{\beta}{r_o}\left(\frac{m}{C_D \rho_o A \alpha}\right)^2 \\
J &= \frac{\sqrt{I \beta r_o}}{2}\left(\frac{L}{D}\right)
\end{aligned}
\right\} \qquad (3)
$$

and

$$
V_E \cong \sqrt{g r_o} = \text{satellite speed}
$$

The variables of equation (2) are closely related to those of the motion analyses of reference 1 for ballistic vehicles and reference 2 for glide vehicles. The equation is complicated by its nonlinearity; however, a redeeming feature is that it normalizes with the transformation to the new independent variable $f/\sqrt{I}$. Accordingly, a solution for any set of values of I and J generalizes to other values of I under the same conditions of $f_E/\sqrt{I} = \sqrt{r_o/\beta}\,(C_D \rho_E A/m)$, $(1/\sqrt{I})(df/dZ)_E = \sqrt{\beta r_o}\,\theta_E$, and $\sqrt{\beta r_o}\,(L/D)$. Thus, for example, shape, size, and mass of a ballistic vehicle (J = 0) determine primarily the altitudes at which major decelerations occur, but not the magnitude of these decelerations. This result is identical to that of reference 1 for ballistic missiles entering the atmosphere at relatively large angles.

In the case of ballistic satellite re-entry a numerical solution to equation (2) is required when θ_E, the trajectory inclination at the beginning of re-entry, approaches zero. On the other hand, the family of solutions to equation (2)

$$
f = \sum_{i=o}^{n} a_i Z^i \qquad (4)
$$

is useful provided θ_E does not approach zero. It will be sufficient in the event θ_E is of the order of 2^o or more (negative) to retain only the first two terms of the series, thus

$$
f = \frac{\beta m \theta_E}{C_D \rho_o A \alpha} Z\left(1 - \frac{k}{2} Z\right) \qquad (5)
$$

where

$$k = \frac{1}{\beta r_o \theta_E^2}$$

and should be of the order of 1 or less. In this case the deceleration history

$$-\frac{1}{g}\frac{dV}{dt} = \frac{C_D \rho_o A r_o^{\alpha}}{2m} f e^Z \tag{6}$$

takes the form

$$-\frac{1}{g}\frac{dV}{dt} = \frac{\beta r_o \theta_E}{2} Z\left(1 - \frac{k}{2} Z\right) e^Z \tag{7}$$

which yields

$$\left.\begin{aligned} \left(-\frac{1}{g}\frac{dV}{dt}\right)_{max} &= -\frac{1}{2\theta_E}\left(1 + \sqrt{\frac{1}{k^2} + 1}\right) e^{\left[\frac{1}{k} - 1 - \sqrt{\left(\frac{1}{k}\right)^2 + 1}\right]} \\ \text{at} \quad Z &= \frac{1}{k}\left(1 - k - \sqrt{1 + k^2}\right) \end{aligned}\right\} \tag{8}$$

For values of k small compared to 1 we have

$$\left(-\frac{1}{g}\frac{dV}{dt}\right)_{max} \longrightarrow -\frac{\beta r_o \theta_E}{2e} \tag{9}$$

which is the result of reference 1 for $\theta_E \approx \sin \theta_E$. Range covered during re-entry follows from equation (6) since $\varphi = s/r_o$ where s is range and

$$-\frac{1}{g}\frac{dV}{dt} = -\frac{1}{2} e^Z \frac{dZ}{d\varphi}$$

Thus,

$$-\frac{dZ}{d\varphi} = \beta r_o \theta_E Z \left(1 - \frac{k}{2} Z\right) \tag{10}$$

so we obtain

$$\varphi = \frac{-1}{\beta r_o \theta_E} \ln \left[\left(\frac{Z}{Z_E}\right) \left(\frac{1 - \frac{k}{2} Z_E}{1 - \frac{k}{2} Z}\right) \right] \tag{11}$$

and in the limiting case of $k \ll 1$ we verify the linear trajectory assumption of reference 1, namely

$$\varphi = \frac{-1}{\theta_E} \left(y_E - y\right) \tag{12}$$

These, then, are the motion equations which will be used in the study of ballistic re-entry. Next consider the motion in gliding re-entry.

Equation (2) will give a wide variety of solutions to gliding re-entry; however, it will suffice for most of our purposes to consider the particular case of equilibrium gliding flight. This type of flight is classically defined according to Sänger (ref. 9) as the case where lift plus centrifugal force just counterbalances weight. If the re-entry motion of a satellite is initiated to satisfy these conditions, then equation (2) reduces to the algebraic expression

$$f = -\frac{I}{J} \left(1 - e^{-Z}\right) \tag{13}$$

connecting flight altitude to flight velocity, while range can be related to velocity according to reference 2 as follows

$$\varphi = \frac{1}{2} \left(\frac{L}{D}\right) \ln \left(\frac{1 - e^{Z}}{1 - e^{Z_E}}\right) \tag{14}$$

Maximum deceleration occurs when lift and hence drag are a maximum which is the case at low speeds and low altitudes where centrifugal force becomes relatively small. Thus, while in general from equation (13)

$$-\frac{1}{g}\frac{dV}{dt} = \frac{D}{L}\left(1 - e^{Z}\right) \tag{15}$$

we obtain as Z becomes large negatively

$$\left(-\frac{1}{g}\frac{dV}{dt}\right)_{max} = \frac{D}{L} \tag{16}$$

If the resultant aerodynamic force $\sqrt{D^2+L^2}$ had been employed in this calculation, we would have obtained an effective deceleration

$$G = \frac{\sqrt{D^2+L^2}}{W} = \sqrt{1 + \left(\frac{D}{L}\right)^2}\left(1 - e^{Z}\right) \tag{17}$$

so that

$$G_{max} = \sqrt{1 + \left(\frac{D}{L}\right)^2} \tag{18}$$

which includes the "1g" of steady level flight at low speeds and high L/D.

Heating.- In the following studies of aerodynamic heating, convective heat transfer only will be considered. This simplification is suggested by presently available evidence (ref. 10) which indicates that radiative heat transfer from the hot air envelope about a body should be relatively small in the low-density atmosphere at the high altitudes where a satellite does most of its decelerating.

The "cool-body" and "equilibrium flow" assumptions will be employed in all heat-transfer calculations. Convective heating in the stagnation region will be analyzed by the method of reference 11 which yields results in good agreement with experiment at the enthalpies of hypervelocity flight. In cases where comparative heating is of primary interest, heat transfer to surfaces aft of the stagnation region will be calculated using a simplified ideal gas model of the flow. In particular cases where a somewhat more precise knowledge of heating is required, heat transfer to these surfaces will be calculated by the method of Lees (ref. 12).

Assuming laminar boundary-layer flow we can write for the average or local heat-transfer rate

$$q = C\sqrt{\frac{\rho}{x}}\,V^3 \tag{19}$$

where C is a constant depending on body shape and gas properties, ρ is ambient air density, and x is a body dimension. In the notation of our motion analysis this equation becomes

$$q = \frac{C}{x^{1/2}} (\alpha\rho_o)^{1/2} (gr_o)^{3/2} f^{1/2} e^{3Z/2} \tag{20}$$

which can be evaluated for any $f = f(Z)$ obtained by solution of equation (2).

In the case of ballistic re-entry at small but finite θ_E we have then from equation (5)

$$\left.\begin{aligned} q &= K_1 \left[-Z\left(1 - \frac{k}{2} Z\right)\right]^{1/2} e^{3Z/2} \\ \text{where} \qquad K_1 &= C(gr_o)^{3/2} \left(\frac{-\beta m \theta_E}{C_D A x}\right)^{1/2} \end{aligned}\right\} \tag{21}$$

Accordingly, maximum heating rate is

$$q_{max} = \frac{K_1}{3} \left(k + \sqrt{9 + k^2}\right)^{1/2} e^{\frac{3}{2k}\left[1 - \frac{k}{3} - \sqrt{1 + \left(\frac{k}{3}\right)^2}\right]} \tag{22}$$

and it occurs when

$$Z = \frac{1}{k}\left[1 - \frac{k}{3} - \sqrt{1 + \left(\frac{k}{3}\right)^2}\right] \tag{23}$$

Equilibrium surface temperatures for a radiation-cooled vehicle follow from equation (21) or (22) and the Stefan-Boltzmann law, thus

$$T_{RE} = \left(\frac{q}{\epsilon\lambda}\right)^{1/4} \tag{24}$$

where ϵ is surface emissivity and λ is the Stefan-Boltzmann constant.

In order to evaluate the heat convected to a vehicle during ballistic re-entry it is useful to note that $q = dH/dt = \sqrt{g/r_o}\, e^{Z/2}(dH/d\varphi)$. With this information equations (5), (10), and (20) combine to yield

$$\left.\begin{aligned} dH &= -K_2 \frac{e^Z dZ}{(-Z)^{1/2}\left(1 - \frac{k}{2} Z\right)^{1/2}} \\ \text{where} \quad K_2 &= \frac{C g r_o}{(-\beta\theta_E)^{1/2}}\left(\frac{m}{C_D A x}\right)^{1/2} \end{aligned}\right\} \qquad (25)$$

Now we note that the large majority of convective heating takes place in the range of Z from 0 to the order of -1. Accordingly, to the accuracy of this equation we can write

$$dH = -K_2 \frac{e^Z}{(-Z)^{1/2}}\left(1 + \frac{k}{4} Z\right) dZ$$

which yields for heat convected during re-entry

$$H = \sqrt{\pi}\, K_2 \left(1 - \frac{k}{8}\right) \qquad (26)$$

In the case of ballistic re-entry at values of θ_E approaching zero the previous analytic results for heating do not in general apply, and numerical methods will be employed to obtain maximum heating rates and integrated heat transfer from equation (20).

In the case of equilibrium gliding re-entry we have from reference 2 for laminar flow that the expression for heating rate can be written

$$\left.\begin{aligned} q &= K_3 \left(1 - e^Z\right)^{1/2} e^Z \\ \text{where} \quad K_3 &= C g r_o \sqrt{\frac{2m}{C_L A x}} \end{aligned}\right\} \qquad (27)$$

and maximum heating rate is

$$q_{max} = \frac{2}{3\sqrt{3}} K_3 \tag{28}$$

which occurs when

$$Z = \ln \frac{2}{3} \tag{29}$$

In the case of a radiation-cooled vehicle equilibrium surface temperatures are again given by equation (24) using values of q from equations (27) and (28).

The heat convected to a glide vehicle during re-entry is calculated by a procedure entirely analogous to that employed for ballistic vehicles (see development of eqs. (25) and (26)). Thus we obtain

$$H = K_4 \left\{ \frac{1}{2} \left[\frac{\pi}{2} - \sin^{-1} \left(2e^Z - 1 \right) \right] + \sqrt{e^Z \left(1 - e^Z \right)} \right\} \tag{30}$$

which becomes as $Z \to -\infty$

$$\left. \begin{aligned} H &= \frac{\pi}{2} K_4 \\ \text{where} \quad K_4 &= \frac{C}{\sqrt{2}} (g r_o^3)^{1/2} \left(\frac{L}{D} \right) \sqrt{\frac{mg}{C_L A x}} \end{aligned} \right\} \tag{31}$$

Application of analysis.- It will be convenient to employ essentially conical vehicles in studying general features of motion and heating during re-entry, because the calculations are simplified without obscuring the roles of important variables. In addition, we will be interested primarily in shapes which develop pressure forces that are large by comparison to viscous forces, and so the latter forces will be neglected in estimating lift and drag during re-entry.

Accordingly, if the ballistic vehicle is a right circular cone with modest nose bluntness we have approximately from Newtonian theory that

$$C_D = 2 \sin^2\delta \tag{32}$$

where δ is the half-cone angle. Removing the top half of the cone yields a glide vehicle of the same drag coefficient and the following lift coefficient

$$C_L = \frac{4}{\pi} \sin \delta \cos \delta \tag{33}$$

so that the lift-drag ratio is

$$\frac{L}{D} = \frac{2}{\pi} \frac{1}{\tan \delta} \tag{34}$$

In the general heating study we will need the values of the constants C appearing in the heating-rate and integrated heat-transfer equations. From the results of reference 11 we can define the value of C_S in the stagnation region of a blunt nose. Thus setting $X = \sigma$ where σ is the radius of curvature of the blunt nose, we have

$$C_S = 1.36 \times 10^{-5} \text{ slugs}^{1/2}/\text{ft} \tag{35}$$

which includes a conservative estimate of the effects of equilibrium dissociation. In evaluating heating of the cone aft of the blunt nose we will set $X = r_b$, where r_b is the radius of the base of the cone, and use the average constant

$$C_a = 1.03 \times 10^{-5} \sin \delta \cos^{1/2}\delta \text{ slugs}^{1/2}/\text{ft} \tag{36}$$

obtained in the manner of appendix B with the assumption of ideal gas flow. This assumption appears justified on the basis of reference 12, so long as surface inclinations are not too close to the vertical. We will neglect heating of the base of a body in all cases, and will neglect heating of the flat top of the half-cone glide vehicles in comparative studies.

Heating rates and integrated heat transfer per unit area are obtained directly from the equations developed in the heating analysis and the constants given above. In order to obtain total heat transfer to ballistic and glide vehicles, frontal surface area S must be known. In the case of right circular cones this area is related to base area A and cone angle δ by the expression

$$S = \frac{A}{\sin \delta} \tag{37}$$

Thus total heat transfer Q is

$$Q = HS \tag{38}$$

where H for the ballistic vehicle is given by equation (26) and for the glide vehicle it follows from equation (31).

In calculating the radiation-equilibrium temperatures, a value of 1.0 will be taken for ϵ, and 0.373×10^{-9} ft-lb/ft^2-sec for λ.

Discussion of General Features of Motion and Heating

The analytical results just described will now be used to investigate some general features of ballistic and gliding re-entry.

Ballistic re-entry.- The calculated effect of entry angle on maximum deceleration is shown in figure 3. It is indicated that near zero entry angle this deceleration is about 8 g's. Note, however, that maximum deceleration increases rapidly with entry angle for angles in excess of a degree or so.

We inquire next about the convective heating of ballistic vehicles during atmospheric entry. Laminar flow was assumed in analyzing this heating and it is necessary to justify this assumption. This can be done by noting that the Reynolds number per foot under conditions of maximum heating rate (see eqs. (5) and (23)) is given for k of the order of 1 or less by the expression

$$\left(\frac{Re}{l}\right)_{q_{max}} = \frac{\beta \sqrt{g r_o}}{\mu_o} \left(\frac{m}{C_D A}\right) \theta_E Z \left(1 - \frac{k}{2} Z\right) e^{Z/2}$$

where

$$Z = \frac{1}{k}\left[1 - \frac{k}{3} - \sqrt{1 + \left(\frac{k}{3}\right)^2}\right]$$

With these equations and the results of numerical calculations for the case of k greater than 1, we obtain the Reynolds numbers shown in figure 4. Thus if $m/C_D A$ is the order of 1, $(Re/l)_{q_{max}}$ is the order of 10^5

for the small θ_E of principal interest to us, and so laminar flow should be practical to obtain on vehicles of not too large size.

The calculated laminar heating of conical ballistic vehicles entering the earth's atmosphere at negligible angle to the horizontal is shown in figure 5 for vehicles of various weights all having the same base area of 25 square feet. Initial values of $f/\sqrt{I}$ and Z equal to zero were employed in calculating these results.[2] The values of α and β in the exponential altitude-density relationship were chosen with particular attention to the altitude range from 0 to 100 miles (see appendix A and fig. 24) where most of the convective heating occurs. Figure 5 shows that both total and stagnation-point heat transfer are substantially reduced by employing high drag (in this case high cone angle) shapes which impart most of their kinetic energy to the atmosphere in the form of heat. This trend was first noted in reference 1 in connection with ballistic missile studies. Maximum radiation-equilibrium temperatures for these cones are shown in figure 6. It is not surprising that these temperatures decrease with increasing cone angle since they are determined by heating rates which are proportional to heat transfer Q. It is indicated that the light weight cones have average equilibrium temperatures of the order of 3000° R and less, whereas the stagnation-region temperatures can be reduced to this order only by increasing the radius of curvature of the surface above 1 foot.

The effect of entry angle on the heating of conical ballistic vehicles shown in figure 7 was calculated with the assumption that $f/\sqrt{I}$ and Z are initially zero.[3] It is seen that increasing the entry angle substantially reduces net heat transfer, while the maximum heating rates and hence equilibrium temperatures are substantially increased. Thus with a heat-sink design higher re-entry angles may be advantageous, whereas with a radiation-cooled design it appears desirable to keep the re-entry angles as low as possible.

Gliding re-entry.- We will consider now the effect of lift on re-entry, and we will focus attention primarily on the equilibrium glide trajectory. The decelerations in equilibrium gliding flight approach a maximum with decreasing altitude and speed, and the effect of lift-drag ratio on maximum deceleration is given by equation (16) as

---

[2]For values of Z near zero the solution $f = (2\sqrt{I}/\sqrt{3})(-Z)^{3/2}$ to equation (2) was employed in these calculations.

[3]Note that the curve for integrated heat transfer $H/H_{\theta_E=0}$ is strongly dependent on the initial condition of integration. Thus for example, at $\theta_E = 0^{\circ}$ the net heat transfer for $Z_i = -0.02$ $(V_i/V_E = 0.99)$ is about 60 percent of that for $Z_i = 0$ $(V_i/V_E = 1.0)$ while at $\theta_E = -2^{\circ}$, the net heat transfer for $Z_i = -0.02$ is about 80 percent of that for $Z_i = 0$.

$$\left(-\frac{1}{g}\frac{dV}{dt}\right)_{max} = \frac{D}{L}$$

It is clear from this relation that even small lift-drag ratios, for example of the order of 1/2, markedly reduce maximum deceleration below that experienced by a ballistic vehicle. Note too that with increasing lift-drag ratio the maximum decelerations rapidly approach those of conventional airplane flights. Equation (16) overestimates deceleration at lift-drag ratios near zero. Under these circumstances a more accurate estimate of maximum decelerations may be obtained by numerical integration of equation (2) (see fig. 8 and also ref. 6).

In the analysis of heating in gliding flight it was assumed, just as in ballistic flight, that the boundary layer was laminar. This assumption can be justified by noting that the Reynolds number per foot under conditions of maximum heating rate (see eqs. (13) and (29)) is given by the expression

$$\left(\frac{Re}{l}\right)_{q_{max}} = 2.83\times10^{3}\,\frac{m/C_DA}{L/D} = 2.83\times10^{3}\,\frac{m}{C_LA}$$

Comparison of Reynolds numbers predicted by this expression with those for ballistic re-entry shows that for comparable m/C_DA and lift-drag ratios of any consequence, gliding re-entry is characterized by substantially lower Reynolds numbers. Accordingly all laminar flow should be even more readily obtained in the case of gliding re-entry than in the case of ballistic re-entry.

Now the glide vehicle was assumed to be a half-cone at zero angle of attack relative to the top surface. This choice of shape simplifies the calculations and facilitates the comparison of heating results with those obtained for conical ballistic vehicles. The lift and drag of half-cones (see eqs. (32) to (34)) are shown in figure 9. It is seen that lift-drag ratios decrease from 2 down to 1/4 as the cone angle is increased from 20° to 70°. Note too that lift coefficient is a maximum at 45° cone angle, while drag coefficient increases monotonically with increasing cone angle. These estimated aerodynamic characteristics have been used in the calculations of the total and stagnation-point heating of conical glide vehicles shown in figure 10; it was again assumed that all vehicles have the same base area of 25 square feet. We see that with increasing cone angle, and hence decreasing L/D, heat transfer is substantially decreased. This result is connected, of course, very closely with the effect of increasing cone angle to decrease heating of ballistic vehicles. The effect of cone angle on maximum equilibrium temperatures of conical glide vehicles is shown in figure 11. The variation of stagnation temperature with cone angle is a direct consequence

of the variation of lift coefficient with cone angle (see eqs. (27), (28), and (35) showing that $q \sim \sqrt{1/C_L} \sim \sqrt{1/\sin \delta \cos \delta} \sim T^4$). The tendency of average temperature to increase somewhat with cone angle is traceable largely to the increased "wing" loading associated with increased cone angle (see eqs. (27), (33), and (36)).

Comparative heating of ballistic and glide vehicles.- We can put these results in a generalized form which permits an interesting comparison between the heating of conical ballistic and glide vehicles. This comparison is made in figure 12, and it will be helpful to remember that when these vehicles have the same cone angle they have the same drag coefficient. Note first that so far as average and stagnation-point heating is concerned the ballistic vehicle is superior to the glide vehicle. On the other hand so far as radiation-equilibrium temperatures are concerned the glide vehicle is superior to the ballistic vehicle. Accordingly we can reach the general conclusion that ballistic vehicles are likely to be better for heat-sink designs while glide vehicles are likely to be better for radiation-cooled designs.[4]

However, the high cone angle, low L/D glide vehicle is not grossly inferior to the ballistic vehicle as a heat-sink design and moreover there is the attractive possibility of making the glide vehicle a combination heat-sink, radiation-cooled design, thereby substantially reducing heat-shield weight. We recognize too that the lift developed by the glide vehicle offers advantages over the ballistic vehicle in terms of reduced decelerations and increased maneuverability during re-entry. These advantages become especially significant when the re-entry of a manned vehicle is considered which is the matter we will now investigate.

A MANNED RE-ENTRY VEHICLE

We inquire, specifically, if a half body of the type we have been discussing can be converted into a practical flying machine in which the man plays an active role during re-entry as well as orbiting flight. We have seen that the asymmetry of a large angle half-cone provides it with the combined capability of high lift to reduce heating rates, and high drag to reduce total heating. In addition, the flare of the body tends to give it inherent static stability. A more careful consideration of the factors of heating, deceleration, and stability leads us to choose a modified 30° semiapex angle cone for the basic study shape as shown in figure 13. A configuration with a larger cone angle would, of course,

[4]Application of ablation cooling techniques to satellites requires further study; however, preliminary indications are that these techniques will tend to be better suited to ballistic vehicles because they tend to experience higher heating rates and shorter heating times than glide vehicles.

have a smaller amount of heat convected to it during re-entry. However, the configuration would tend to have less satisfactory dynamic stability characteristics and would experience higher decelerations during re-entry than the configuration chosen. The body was made slightly larger than a half-cone to provide more usable depth for a given length; corners and nose have been rounded to reduce local heat-transfer rates, and trailing-edge flaps have been provided for longitudinal and lateral control. Drag can be increased by flaring all controls simultaneously which provides a method for varying the longitudinal glide range. The aspect ratio of the controls was kept low (0.6) to minimize the effects of shock-wave boundary-layer interaction and Mach number on control effectiveness.

Aerodynamic Characteristics

To calculate the aerodynamic characteristics of this configuration Newtonian impact theory was used for the nose, conical surface, and controls; two-dimensional shock-expansion theory was used for the top surface; and the pressure coefficient on the base was assumed to be 0.7 of the vacuum pressure coefficient. Calculations were made for Mach numbers 3 to 6 and ∞. The calculations indicated that the configuration would be statically stable and controllable at supersonic speeds.

A series of wind-tunnel tests was conducted to check these estimates and to determine the static stability and control characteristics of the configuration at subsonic and low supersonic speeds. These tests were conducted in Ames Laboratory wind tunnels at the Mach numbers and Reynolds numbers (based on body diameter) given in the following table:

Wind tunnel	Mach number	Reynolds number, million
12-foot	0.25	0.6
6- by 6-foot	0.6 to 2.2	0.65
10- by 14-inch	3.0 (air)	0.43
	4.0 (air)	1.82
	5.0 (air)	.79
	6.0 (air)	.38
	12.2 helium	.56

Detailed descriptions of the wind tunnels may be found in references 13, 14, and 15. A representative portion of the experimental results will be shown. All force and moment coefficients are referenced to the body

base area ($A = 1.26\ l^2$), pitching-moment coefficients are referred to body length, and yawing- and rolling-moment coefficients to body diameter.

Performance.- The calculated and experimental values of trim lift coefficient and lift-drag ratios are shown in figure 14. At $M = 3$ and above, the configuration self-trims (i.e., with controls undeflected) at an angle of attack of about 4° measured with respect to the top surface of the body. Also at Mach number 3 and above, theory and experiment are in good agreement. At these speeds, little variation with Mach number is observed, and the calculated values at $M = \infty$ are very close to the values obtained at $M = 3$ to 6.

The configuration could, therefore, glide at a constant lift coefficient of about 0.36 and a constant lift-drag ratio of about 0.5 throughout most of the re-entry. The maximum deceleration would not, in this case, exceed about 2 g's in the glide. Experimental data for this configuration were obtained up to a Mach number of 6. A test of a similar configuration having a small wing at Mach numbers from 3 to 12.2 also showed very little change in aerodynamic characteristics at Mach numbers greater than 4. At Mach numbers below 2, the configuration under study here is not self-trimming. At these speeds, the configuration was trimmed with lower controls deflected. The maximum control deflection used was about 45° at $M = 0.25$.

Static stability and control characteristics.- The static stability characteristics at trim lift are presented in figure 15. Values for longitudinal stability, C_{m_α}, directional stability, C_{n_β}, and dihedral effect, C_{l_β}, are shown as functions of Mach number. The results indicate that the configuration is stable about all three axes and at all test Mach numbers. Again at $M = 3$ and above, theory and experiment are in good agreement, little variation with Mach number is noted, and all measured values are close to the estimated $M = \infty$ values.

High-speed control characteristics evaluated at the self-trimmed angle of attack are given in figure 16. Incremental changes in forces and moments with changes in control deflection are given. Moments with flaps deflected as ailerons are shown in figure 16(a) and forces and moments with flaps deflected as elevators are shown in figure 16(b). The control effectiveness is, in general, fairly well estimated by the Newtonian impact theory. Thus, the effects of Mach number and shock-wave boundary-layer interaction apparently are of minor significance. Preliminary calculations indicate that these controls should, in general, have adequate effectiveness at dynamic pressures as low as 7 pounds per square foot.

It is evident from figures 16(a) and 16(b) that aileron deflection of the upper controls would also produce considerable changes in pitching and yawing moments, and a large amount of undesirable cross-coupling

of motions could result. As shown in figure 16(c), if the lower control is deflected differentially along with the upper control such that the pitching moments are cancelled, most of the yaw due to aileron would also be cancelled up to deflection angles of about 40° for the upper control. Thus, aerodynamic cross-coupling can be eliminated for aileron deflections less than 40° at supersonic speeds.[5]

As mentioned previously, drag can be increased by flaring all controls simultaneously. We see that the upper controls deflected 60° and the lower controls deflected about 35° have lift and moment increments which are approximately equal and of opposite sign. With controls in this position the trimmed lift coefficient remains about the same; however, the lift-drag ratio is reduced about 10 percent. This reduction in L/D yields about a 10-percent reduction in longitudinal glide range which could be used to adjust the longitudinal location of the landing point. Comparable reductions in L/D and hence glide range can also be achieved by changing the angle of attack of the vehicle.

The results of this investigation indicate then that a vehicle of the proposed shape can be made statically stable and controllable throughout the re-entry speed range. It is appropriate, therefore, to take a closer look at the motion and aerodynamic heating encountered during re-entry.

Re-entry Trajectory and Heating

To calculate the trajectory, a total re-entry weight of 4000 pounds and a body length of 6-2/3 feet were assumed for the vehicle. The vehicle was considered to be in a circular orbit at an altitude of 100 statute miles, and it was assumed that reverse thrust was used in accordance with the method of appendix C to bring the vehicle down to an altitude at which aerodynamic drag becomes significant. From this altitude the vehicle followed essentially the equilibrium glide path if the reverse thrust was small, or an oscillatory path if the reverse thrust was large. Let us consider first the motion and heating encountered in the equilibrium glide trajectory.

Equilibrium glide.- The variations of altitude and flight velocity with distance traveled during re-entry are shown in figure 17. A reverse thrust of 4.24 pounds acting over a period of 47 minutes was assumed in calculating this trajectory. The flight path angle at the end of reverse thrust is small, about 0.2° with respect to the local horizontal, and the vehicle follows essentially an equilibrium glide trajectory. The total re-entry range is about 20,000 miles. It is apparent that the flight

[5]Yaw flaps located on the sides of the body may also prove desirable to provide independent yaw control over the speed range.

velocity remains close to satellite speed over 80 percent of the total range and that the glide phase amounts to about 1/3 of the total range. The total time of descent is 76 minutes.

The convective heating experienced by the vehicle for this trajectory is shown in figure 18. The rate of heating of various portions of the body is shown as a function of distance traveled. We can see that most of the heating occurs in the last half of the glide phase. The peak stagnation-region heating rate of about 71 Btu per square foot per second occurs at an altitude of about 43 miles and a velocity of 22,500 feet per second. Average heat rates to the bottom and top surfaces are about 1/4 and 1/20 the stagnation-region value, respectively. The total amount of heat convected to this configuration is of the order of 1.6×10^6 Btu's for the entire period of descent.

Oscillatory glide.- If the amount of reverse thrust is larger, the vehicle follows an oscillatory trajectory as shown in figure 19 and calculated with equation (2). The reverse thrust employed for this trajectory was 71 pounds acting over a period of 18 minutes. At the end of reverse thrust, the flight path angle is about $1\text{-}1/2^\circ$ with respect to the local horizontal. There are no appreciable fluctuations in velocity from that in the equilibrium glide, and the maximum accelerations do not exceed that in the equilibrium glide. However, there are some significant variations in altitude and at the bottom of the first oscillation the altitude is about 3 miles below that for the vehicle in an equilibrium glide.

The stagnation-region heating experienced by the vehicle in this oscillatory trajectory is shown in figure 20. The maximum stagnation-point heating rate which occurs near the bottom of the first oscillation is about 100 Btu's per square foot per second which is about 40 percent higher than the value obtained for the equilibrium glide trajectory. While the heat rates are higher, the flight time is less and the total heat load is 1.5×10^6 Btu's, about the same as for the equilibrium glide of figure 18. With this information on heating we are in a position to give some consideration to the structure of the vehicle.

Structure

Figure 21 shows a sketch of the pertinent details of a possible structural arrangement. Note first that the man and all internal equipment are contained in a capsule. The capsule is protected from the effects of aerodynamic heating by an external heat shield to which it is attached at the base of the configuration. As shown in the detail, the capsule is separated from the heat shield by an air gap, a light-weight radiation shield of metallic foil, and a blanket of low-density

insulation. Heat transfer to the capsule is thereby minimized, and the problem of maintaining it hermetically sealed and air conditioned should be simplified.

The maximum temperature of the heat shield must not, of course, exceed the temperature limitations of the shield material. If the heat-sink concept is employed in the relatively low heating-rate environment which is typical of satellites, the maximum material temperature is controlled primarily by the heat capacity and thickness. As indicated in the sketch, the heat-shield thickness tends then to vary in proportion to the heat input at any point on the surface. Beryllium appears suited as a heat-sink material for satellites because it has low density and adequate thermal conductivity to utilize essentially the full advantage of its high heat capacity. From both a structural strength and oxidation standpoint, the maximum allowable temperature of beryllium appears to be about 1650° F (see ref. 16). Based on the total heat load of 1.6 million Btu's and on the thermal properties of beryllium from 40° F up to this temperature, the weight of heat-sink material and hence heat shield required for the vehicle would be about 1300 pounds. The nominal wall thickness would be about 1 inch while the maximum thickness at the stagnation point would be about 4-1/2 inches.

It is immediately evident, of course, that a saving in weight of heat shield could be realized if a substantial fraction of the convective heat load could be radiated back to the atmosphere. For radiation to be effective, however, the surface temperature of the heat shield would have to be substantially raised, especially in the stagnation region. For complete radiation cooling, for example, the maximum surface temperature (for an emissivity of 0.8) would be approximately 3200° F at the stagnation point and from 2700° F down to 2100° F along the conical body. Intermediate temperatures between those for the heat-sink and radiation-cooled heat shields, with consequent reductions in heat-shield weight, can be attained by using an insulated heat-sink construction. This type of construction, as suggested by Ferri, et al. (ref. 4), and by Brooks, Anderson, and Swann in unpublished work at the NACA Langley Laboratory, consists of covering the heat sink with a relatively high-temperature insulating refractory coating. On the basis of theoretical estimates by Brooks, et al., this could probably reduce the heat-shield weight to about 50 percent of that for the simple heat-sink concept.

Study Vehicle

A dimensioned two-view sketch and an approximate weight breakdown of the study vehicle are shown in figure 22. At the top left is shown the approximate position of the pilot and the surrounding internal equipment. The control surfaces and small thrust units for high altitude

orientation and re-entry reverse thrust, and the parachute pack for final recovery extend from the base. The distribution of internal weight is also given in figure 22.

The 1300 pounds of heat shield represents only about 33 percent of the total re-entry weight of 4000 pounds; hence, even the simple heat-sink design appears acceptable from a weight standpoint. If the insulated heat-sink concept proves practical to the extent that the weight of the heat shield can be cut by about 50 percent, then with all other components being the same, the heat-shield weight would be reduced to an attractively low figure of less than 20 percent of the total weight.

As a final point it is of interest to inquire how well a pilot might actually "fly" this vehicle back into the atmosphere. Preliminary calculations were made of the Dutch roll oscillation for the vehicle in an equilibrium glide with values for the aerodynamic damping and cross derivatives estimated according to Newtonian impact theory. The calculations indicated that the oscillation is stable, although lightly damped, and has periods varying from about 5 seconds at a velocity of 25,000 feet per second to a minimum of 1.6 seconds at 5500 feet per second. These periods are the same as those of current manually controlled fighter aircraft and therefore do not imply unacceptably high natural frequencies.

The flyability of the machine was explored with an analog simulator. This simulator contained a human pilot and could be operated either with a fixed base or with two degrees of freedom, that is angular motion in pitch and roll. The pitch control channel was a relatively complete representation based on the measured aerodynamic characteristics of the vehicle. The roll channel response was approximated by a single degree of freedom equation giving the right order of frequency and damping in roll. It should be regarded primarily as a distraction to help the pilot assess the pitch control accurately. The simulator was equipped with a conventional, centrally mounted stick and was flown by experienced NACA test pilots.

The task given the pilots was to make a re-entry at zero roll and yaw, and at constant pitch attitude with respect to the local horizon starting from level flight at 270,000-feet altitude and a speed of 22,000 feet per second. These starting conditions lead to a re-entry trajectory with phugoid or long-period oscillations about the equilibrium glide trajectory and resulting higher dynamic pressures, larger decelerations, and higher short-period-oscillation frequencies (minimum periods of about 0.7 second compared to 1.6 seconds for equilibrium glide). It is evident that this re-entry trajectory will be more difficult to fly than one which more nearly simulates the equilibrium glide trajectory.

The comparison between fixed and moving-base simulation at natural low levels of aerodynamic damping was especially interesting. The

majority of the pilots could not handle the control problem on the fixed-base simulator and, in fact, lost control. However, satisfactory re-entries were made as soon as the simulator was allowed to move. This was because the maximum frequencies of the vehicle were sufficiently low for the pilot to attempt to control the motion (see ref. 17). Therefore, he needed the motion input to his body (vestibular response) in order to have enough anticipation or lead time in his control motions.

Using the moving base simulation the pilots rated control as "marginal" with natural damping and "good" with augmented damping. The absence of cross-control problems or further distractions should be remembered, however. Some of the characteristics of the trajectories flown with natural damping are summarized in figure 23. The maximum normal and longitudinal accelerations are moderate and relatively independent of the pitch attitude commanded by the pilot. These values suggest that centrifuge tests where changes in "g" can be simulated may not be essential for trajectory control studies, although the feasibility of certain control operations in the presence of as much as 4 g's longitudinal acceleration should certainly be checked.

The variation of range with commanded pitch attitude is important because it is a measure of the pilot's ability to control his touchdown point. In these simulated flights the pilot controlled this point over a range of 230 miles with an accuracy of 9 miles by controlling pitch attitude within 1°.

As a final remark it might be noted that all the pilots agreed that for this trajectory the most critical region of flight appeared to be at about 180,000 feet where the vehicle would try to skip if reasonably close control were not maintained. The problem was to prevent the skip without overcontrolling and getting into a self-induced pitch oscillation.

CONCLUDING REMARKS

As a result of this investigation it appears that a high-lift, high-drag configuration resembling a half-cone is attractive for the manned satellite application. Decelerations are low enough to permit the pilot to perform important functions during re-entry as well as orbiting flight. The configuration appears to be stable and controllable down to low subsonic speeds and is sufficiently maneuverable in the atmosphere to allow a lateral deviation of as much as ±320 miles and a longitudinal variation of as much as ±350 miles in the choice of a landing point. Moreover, it appears that this type of configuration has an acceptably low structural weight, even with a simple heat-sink design.

It is not evident at the present time that a conventional landing can be effected in unpowered flight at the low lift-drag ratios (of the

order of 1 and less) at which this configuration operates. Parachute recovery of the complete vehicle is practical, however, at low speeds and low altitudes, although separation of the heat shield from the capsule prior to impact may be desirable.

Ames Research Center
National Aeronautics and Space Administration
Moffett Field, Calif., July 28, 1958

APPENDIX A

NOTATION

A	base area of vehicle, ft^2
b	diameter of vehicle, ft
C	constant in heat-transfer equation, $slug^{1/2}/ft$
c	constant in skin-friction equation
C_D	drag coefficient, $\frac{D}{(1/2)\rho V^2 A}$
C_F	skin-friction coefficient
$C_{F'}$	equivalent skin-friction coefficient
C_L	lift coefficient, $\frac{L}{(1/2)\rho V^2 A}$
C_l	rolling-moment coefficient, $\frac{\text{rolling moment}}{(1/2)\rho V^2 A b}$
C_m	pitching-moment coefficient, $\frac{\text{pitching moment}}{(1/2)\rho V^2 A l}$
C_n	yawing-moment coefficient, $\frac{\text{yawing moment}}{(1/2)\rho V^2 A b}$
C_p	specific heat of air at constant pressure, ft-lb/slug $^\circ R$
C_V	specific heat of air at constant volume, ft-lb/slug $^\circ R$
D	drag, lb
e	Naperian logarithm base
f	dimensionless function of y proportional to density ratio (see eq. (3))
G	resultant acceleration, g's

g	gravitational acceleration, 32.2 ft/sec^2
H	convective heat transferred per unit of area, ft-lb/ft^2
h	slant height of cone, ft
I	dimensionless parameter in motion equation (see eq. (3))
J	$\frac{L}{D}$ parameter in motion equation (see eq. (3))
k	entrance angle parameter for ballistic vehicles (see eq. (5))
L	lift, lb
$\frac{L}{D}$	lift-drag ratio
l	length of vehicle, ft
M	Mach number
m	mass, slugs
N	component of rocket thrust normal to flight path
P	component of rocket thrust parallel to flight path
Q	total convective heat transferred, ft-lb
q	convective heat-transfer rate, ft-lb/ft^{2}sec
Re	Reynolds number
r	distance from center of earth, ft
r_b	base radius of vehicle, ft
r_c	radius of curvature of flight path, ft
r_o	radius of earth, ft
S	frontal surface area, ft^2
s	distance along flight path, ft
T	temperature, $^\circ$R
t	time, sec
T_r	constant in Sutherland's equation, $^\circ$R

[redacted]

V	velocity, ft/sec
V_E	satellite speed, ft/sec
W	weight, lb
x	body dimension, ft
y	altitude, ft
Z	$\ln\left(\frac{V}{V_E}\right)^2$
α	constant in density-altitude relation, 0.715 (see fig. 24)
β	constant in density-altitude relation, $\frac{1}{24,800}$ ft^{-1} (see fig. 24)
γ	ratio of specific heats, $\frac{C_p}{C_v}$
δ	half-cone angle
δ_{a_u}	upper control deflected as an aileron
δ_{a_l}	lower control deflected as an aileron
δ_{e_u}	upper controls deflected as elevators
δ_{e_l}	lower controls deflected as elevators (δ measured from normal to body base, positive outward)
ϵ	emissivity
θ	inclination of flight path to local horizontal (positive upward)
λ	Stefan-Boltzmann constant, 0.373×10^{-9} ft-lb/ft^2sec $^oR^4$
ρ	air density, slugs/ft^3
σ	nose radius of body, ft
φ	angular range, radians

Subscripts

a	average values
E	entry conditions
i	initial conditions
l	local conditions
o	sea level
RE	radiation equilibrium
S	stagnation conditions
α	derivative with respect to angle of attack
β	derivative with respect to angle of sideslip

Superscript

$\overline{\quad}$	dimensionless drag parameter (e.g., $\left(\frac{\overline{C_D A\sigma}}{m}\right) = \frac{C_D A\sigma/m}{1\ ft^3/slug}$, see fig. 12)

APPENDIX B

CALCULATION OF C_a

Assuming a Prandtl number of unity we have for a cool conical wall from Reynolds analogy (ref. 2)

$$\frac{dH_a}{dt} = \frac{1}{4} \rho V^3 C_F' \tag{B1}$$

where

$$C_F' = \frac{1}{S} \int_S C_{F_l} \left(\frac{\rho_l}{\rho}\right)\left(\frac{V_l}{V}\right) dS \tag{B2}$$

and S is heated surface area while the subscript l refers to local conditions just outside the boundary layer. Now for $(M8)^2 \gg 1$ we have the useful approximations

$$\frac{\rho_l}{\rho} = \frac{\gamma+1}{\gamma-1} = 6 \quad \text{for} \quad \gamma = 1.4 \tag{B3}$$

and

$$\frac{V_l}{V} = \cos \delta \tag{B4}$$

In addition, we note that for right circular cones

$$\frac{1}{S} \int_S C_{F_l} dS = \frac{2}{3}\sqrt{3}\, \overline{C}_{F_l} \tag{B5}$$

where $\overline{C}_{F_l}$ is the average friction coefficient of a flat plate having the same length as the slant height of the cone, and having the same local conditions in the flow outside the boundary layer. Thus

$$\overline{C}_{F_l} = \frac{c}{\sqrt{\frac{\rho_l V_l h}{\mu_l}}} \tag{B6}$$

Now if we consider the disturbed air temperature to be so high that it is determined largely by shock compression, then the energy equation yields

$$T_l = \frac{V^2 \sin^2 \delta}{2C_p} \tag{B7}$$

At high temperatures we can also write from Sutherland's equation for viscosity

$$\mu_l = \mu_o \left(\frac{T_o+T_r}{T_o^{3/2}}\right) T_l^{1/2} \tag{B8}$$

or

$$\mu_l = \mu_o \left(\frac{T_o+T_r}{T_o^{3/2}}\right) \frac{V \sin \delta}{\sqrt{2C_p}} \tag{B9}$$

Combining these results and noting that $h = r_b/\sin \delta$ we obtain for equation (B1)

$$\frac{dH_a}{dt} = c \sqrt{\frac{\mu_o}{2\sqrt{2C_pT_o}} \left(\frac{T_o+T_r}{T_o}\right)} \sin \delta (\cos \delta)^{1/2} \sqrt{\frac{\rho}{r_b}} V^3 \tag{B10}$$

from which it follows that

$$C_a = c \sqrt{\frac{\mu_o}{2\sqrt{2C_pT_o}} \left(\frac{T_o+T_r}{T_o}\right)} \sin \delta (\cos \delta)^{1/2} \tag{B11}$$

We will take a conservative value of c of unity and set $T_o = 500^\circ$ R for which $\mu_o = 3.58 \times 10^{-7}$ slugs/ft-sec. With $T_r = 216^\circ$ R and $C_p = 6000$ ft^2/sec^2-$^\circ$R we then obtain

$$C_a = 1.03 \times 10^{-5} \sin \delta (\cos \delta)^{1/2} \text{ slug}^{1/2}/\text{ft} \tag{B12}$$

APPENDIX C

ROCKET BRAKING EQUATIONS

Consider a satellite in orbit about the earth at an altitude some distance above the sensible atmosphere. The problem is to initiate re-entry of the vehicle into the atmosphere by application of rocket thrust. Assuming a nonrotating earth and atmosphere and planar motion of the satellite one can write the equations of motion

$$N + \frac{mV^2}{r_c} = W_o \left(\frac{r_o}{r}\right)^2 \cos\theta \tag{C1}$$

$$m \frac{dV}{dt} = -P - W_o \left(\frac{r_o}{r}\right)^2 \sin\theta \tag{C2}$$

where

$$W = W_o \left(\frac{r_o}{r}\right)^2 \tag{C3}$$

and N and P are the components of rocket thrust in the direction normal (positive outward) and parallel (positive rearward) to the direction of satellite motion, respectively. Now we will set

$$\frac{1}{r_c} = \frac{\cos\theta}{r} - \frac{d\theta}{dS}$$

so that equation (C1) becomes (for $\cos\theta \approx 1$, $\sin\theta \approx \theta$)

$$N - mV^2 \frac{d\theta}{dS} = -\frac{mV^2}{r} + W_o \left(\frac{r_o}{r}\right)^2 \tag{C4}$$

But circular satellite orbits are related by the condition that $rV^2 = \text{const} = r_o V_o^2 = g r_o^2$. So if we impose the requirement that during rocket braking the orbit never departs largely from circular we can write equation (C4) as follows

$$\frac{N}{mV^2} - \frac{d\theta}{dS} = \frac{1}{r}\left(1 - \overline{rV^2}\right) \tag{C5}$$

where

$$\overline{rV^2} = \frac{rV^2}{r_o V_o^2} \tag{C6}$$

To the same order of approximation, and noting that $\theta = dr/dS$, equation (C2) becomes

$$-\left(P + \frac{W\theta}{2}\right) = \frac{mV^2}{2}\frac{d\overline{rV^2}}{dS} \tag{C7}$$

Combining equations (C5) and (C7) then yields

$$\left(2\frac{P}{W} + \theta\right) d\theta = \left[(1 - \overline{rV^2}) - \frac{N}{W}\right] d\overline{rV^2} \tag{C8}$$

and so for constant P/W and N/W there is obtained

$$\left(2\frac{P}{W} + \frac{\theta}{2}\right)\theta = -\frac{1}{2}(1 - \overline{rV^2})^2 - \frac{N}{W}\overline{rV^2} + C_1 \tag{C9}$$

which yields for θ

$$\theta = -2\frac{P}{W} + \sqrt{\left(2\frac{P}{W}\right)^2 - (1-\overline{rV^2})^2 - 2\frac{N}{W}\overline{rV^2} + 2C_1} \tag{C10}$$

Combining this expression with equation (C7) and integrating yields angular range $\varphi = S/r$ in the form

$$\varphi = \sin^{-1}\left[\frac{(1-\overline{rV^2}) - \frac{N}{W}}{\sqrt{\left(\frac{N}{W}\right)^2 + \left(2\frac{P}{W}\right)^2 + 2\left(C_1 - \frac{N}{W}\right)}}\right] + C_2 \tag{C11}$$

where the constants of integration C_1 and C_2 are determined from initial flight conditions. The radial location of the trajectory is obtained from equations (C7) and (C10) noting that $d\varphi = dS/r$, thus

$$r = r_i e^{-2\frac{P}{W}\varphi + \left(\overline{r_i V_i^2} - \overline{rV^2}\right)} \tag{C12}$$

where the subscript i denotes initial flight conditions. These equations apply, of course, in both the powered and unpowered or gravity phases of the descent from satellite orbit.[1] In the gravity phase of descent (N = P = 0) the constants C_1 and C_2 are determined by flight conditions at the beginning of this phase.

If braking is by retro-rocket and the vehicle is initially in circular orbit $\theta_i = \varphi_i = 0$, $C_1 = N/W = 0$, and $C_2 = 0$, thus equations (C10), (C11), and (C12) become

$$\left.\begin{aligned} \varphi &= \sin^{-1}\left[\frac{1}{2}\frac{W}{P}\left(1-\overline{rV^2}\right)\right] \\ \theta &= -2\frac{P}{W}(1-\cos\varphi) \end{aligned}\right\} \qquad (C13)$$

and

$$r = r_i e^{-2\frac{P}{W}(\varphi-\sin\varphi)}$$

[1]Indeed they are applicable to either ascending or descending flight so long as the departures from circular satellite conditions are always small.

REFERENCES

1. Allen, H. Julian, and Eggers, A. J., Jr.: A Study of the Motion and Aerodynamic Heating of Missiles Entering the Earth's Atmosphere at High Supersonic Speeds. NACA TN 4047, 1957.

2. Eggers, A. J., Jr., Allen, H. Julian, and Neice, Stanford E.: A Comparative Analysis of the Performance of Long-Range Hypervelocity Vehicles. NACA TN 4046, 1957.

3. Kemp, N. H., and Riddell, F. R.: Heat Transfer to Satellite Vehicles Re-entering the Atmosphere. Jet Propulsion, vol. 27, no. 2, pt. 1, Feb. 1957, pp. 132-137.

4. Ferri, Antonio, Feldman, Lewis, and Daskin, Walter: The Use of Lift for Re-entry from Satellite Trajectories. Jet Propulsion, vol. 27, no. 11, Nov. 1957, pp. 1184-1191.

5. Gazley, Carl, Jr.: Deceleration and Heating of a Body Entering a Planetary Atmosphere from Space. Rand Rep. P-955, 1957.

6. Chapman, Dean R.: An Approximate Analytical Method for Studying Entry Into Planetary Atmospheres. NACA TN 4276, 1958.

7. Eggers, A. J., Jr.: Performance of Long-Range Hypervelocity Vehicles. Jet Propulsion, vol. 27, no. 11, Nov. 1957, pp. 1147-1151.

8. Allen, H. J.: Hypersonic Flight and the Re-entry Problem (Twenty-First Wright Brothers Lecture). Jour. Aero. Sci., vol. 25, no. 4, April 1958, pp. 217-230.

9. Sänger, E., and Bredt, J.: A Rocket Drive for Long Range Bombers. Bur. of Aeronautics, Navy Dept., Trans. CGD-32, 1947.

10. Keck, James, Kivel, Bennett, and Wentinek, Tunis, Jr.: Emissivity of High Temperature Air. Res. Rep. 8, AVCO Res. Lab., April 1957.

11. Eggers, A. J., Jr., Hansen, C. Frederick, and Cunningham, Bernard E.: Stagnation-Point Heat Transfer to Blunt Shapes in Hypersonic Flight, Including Effects of Yaw. NACA TN 4229, 1958.

12. Lees, Lester: Laminar Heat Transfer Over Blunt-Nosed Bodies at Hypersonic Flight Speeds. Jet Propulsion, vol. 26, no. 4, April 1956, pp. 259-269.

13. Edwards, George G., and Stephenson, Jack D.: Tests of a Triangular Wing of Aspect Ratio 2 in the Ames 12-Foot Pressure Wind Tunnel. I - The Effects of Reynolds Number and Mach Number on the Aerodynamic Characteristics of the Wing With Flap Undeflected. NACA RM A7K05, 1948.

14. Frick, Charles W., and Olson, Robert N.: Flow Studies in the Asymmetric Adjustable Nozzle of the Ames 6- by 6-Foot Supersonic Wind Tunnel. NACA RM A9E24, 1949.

15. Eggers, A. J., Jr., and Nothwang, George J.: The Ames 10- by 14-Inch Supersonic Wind Tunnel. NACA TN 3095, 1954.

16. White, D. W., Jr., and Burke, J. E., ed.: The Metal Beryllium. The American Society for Metals, Cleveland, Ohio, 1955.

17. Cheatham, Donald C.: A Study of the Characteristics of Human-Pilot Control Response to Simulated Aircraft Lateral Motions. NACA Rep. 1197, 1954. (Supersedes NACA RM L52C17)

18. Sterne, T. E., Folkart, B. M., and Schilling, G. F.: An Interim Model Atmosphere Fitted to Preliminary Densities Inferred From U.S.S.R. Satellites. Smithsonian Contributions to Astrophysics, vol. 2, no. 10, "Orbital Data and Preliminary Analyses of Satellites 1957 Alpha and 1957 Beta," 1958.

19. Minzner, R. A., and Ripley, W. S.: The ARDC Model Atmosphere, 1956. Air Force Surveys in Geophysics, no. 86, Geophysics Research Directorate, AFCRC, ARDC, Dec. 1956. (Also available as AF Cambridge Research Center TN 56-204)

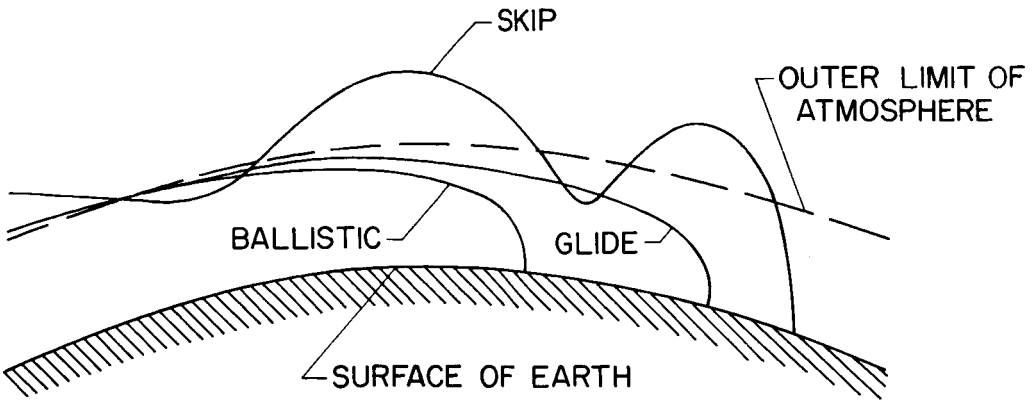

Figure 1.- Re-entry trajectories from satellite orbit.

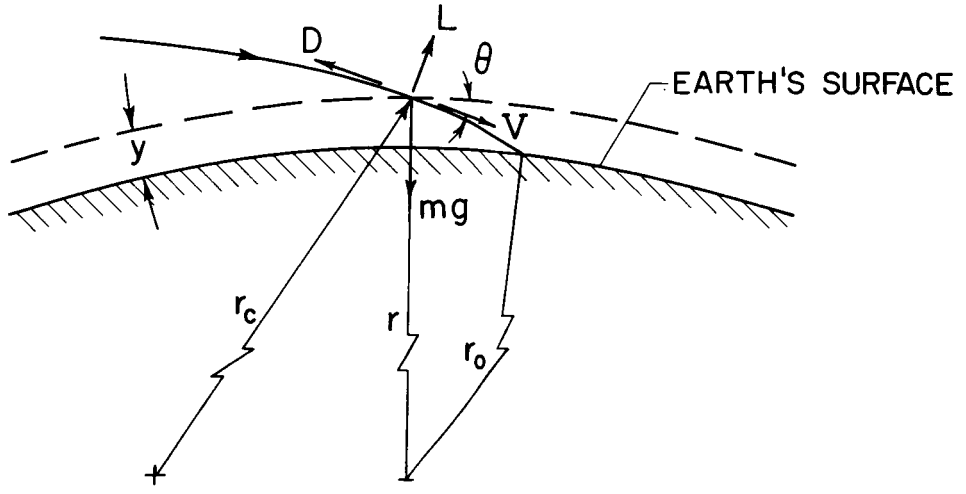

Figure 2.- Notation.

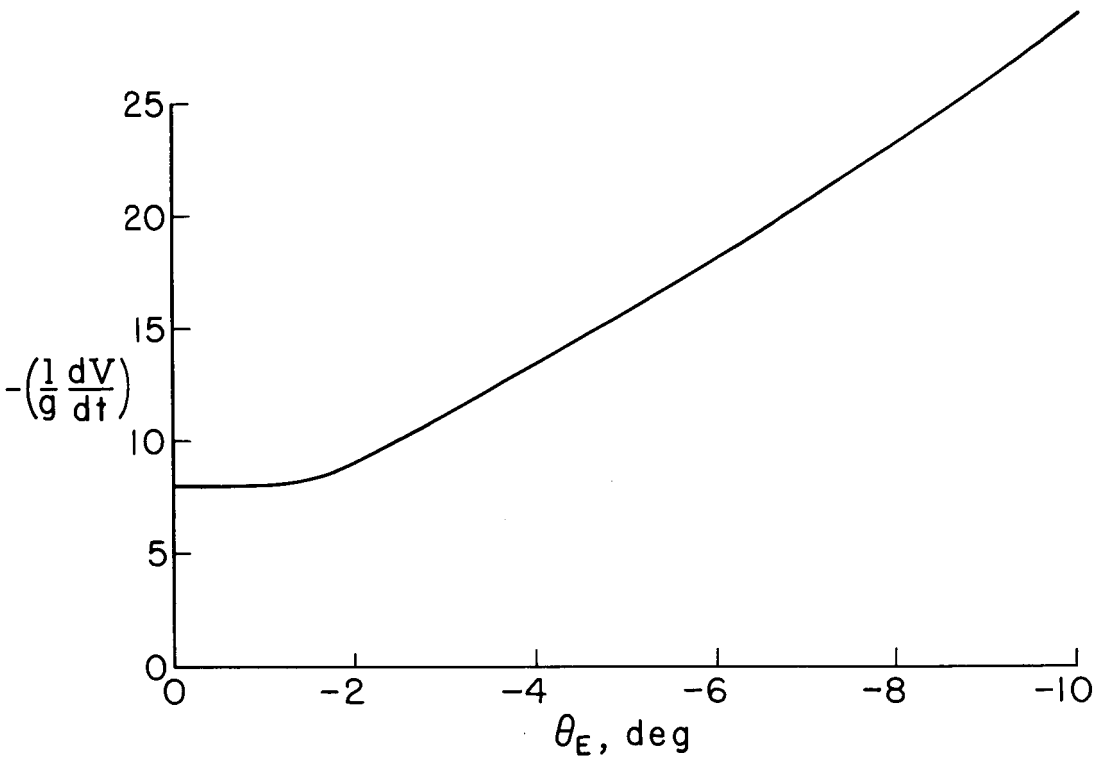

Figure 3.- Effect of re-entry angle on maximum deceleration of ballistic vehicles.

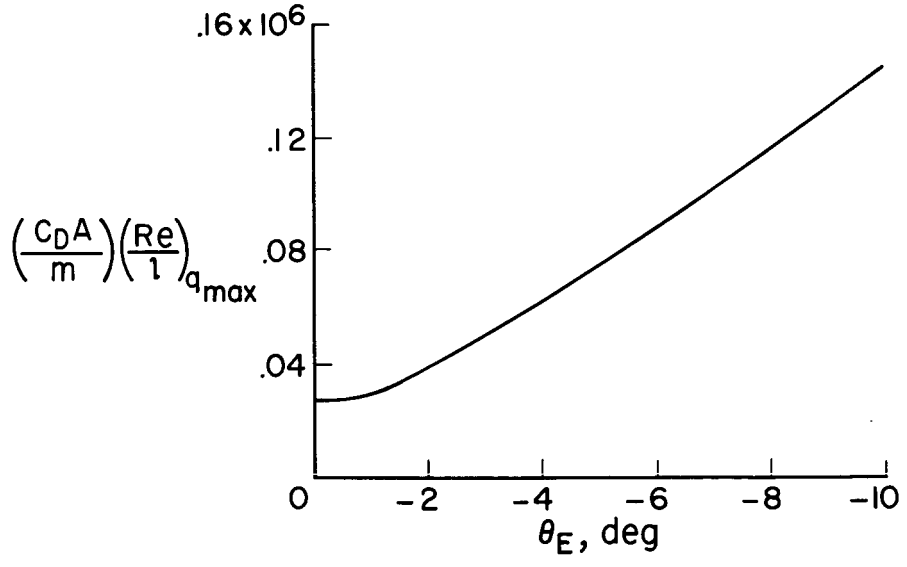

Figure 4.- Effect of re-entry angle on Reynolds number at maximum heating of ballistic vehicles.

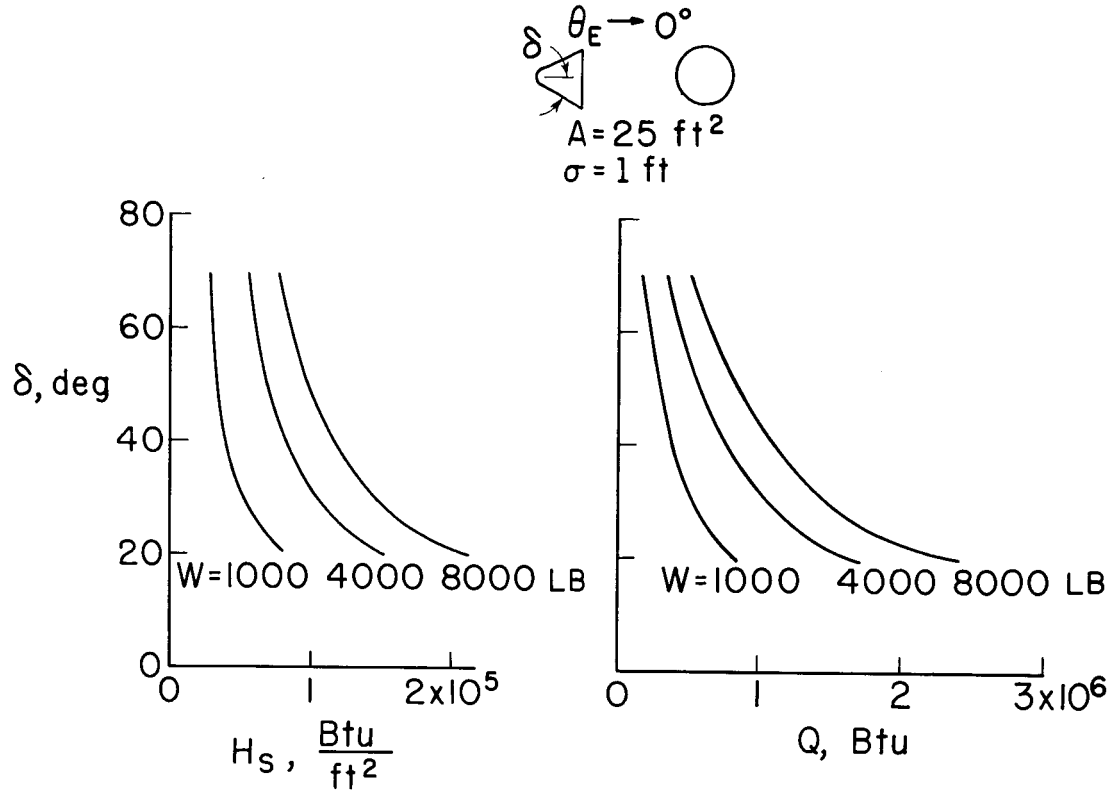

Figure 5.- Heating of conical ballistic vehicles during re-entry.

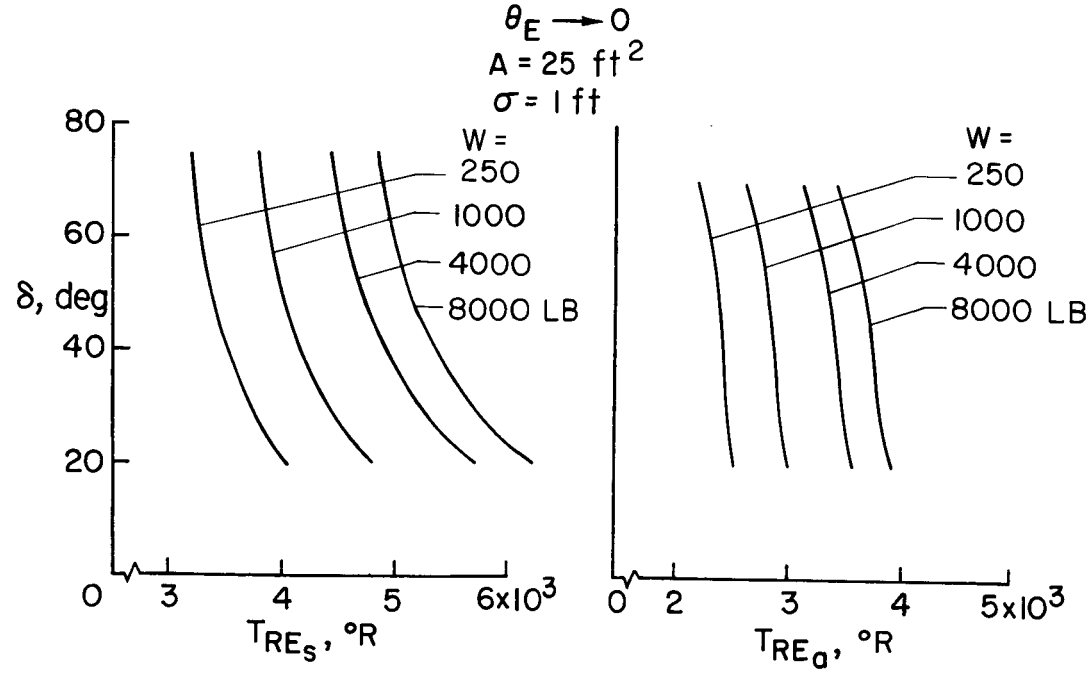

Figure 6.- Maximum radiation equilibrium temperatures of conical ballistic vehicles.

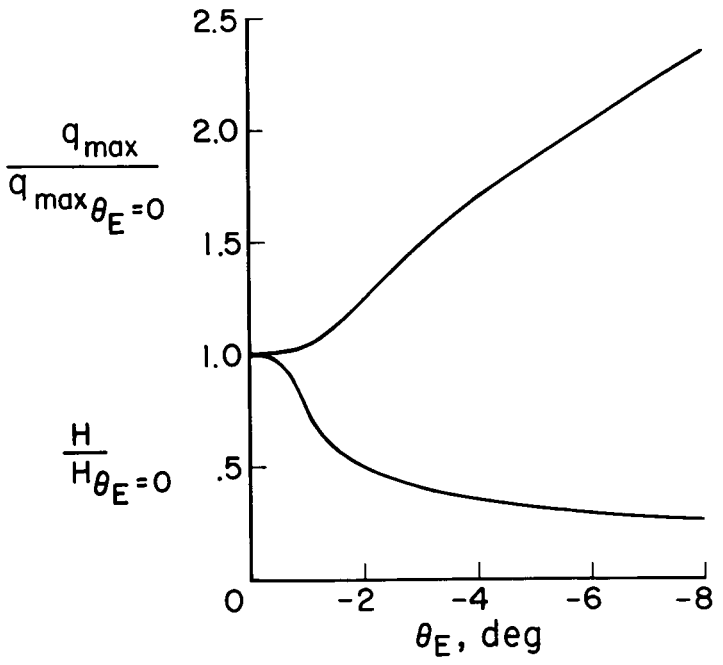

Figure 7.- Effect of re-entry angle on heating of ballistic vehicles.

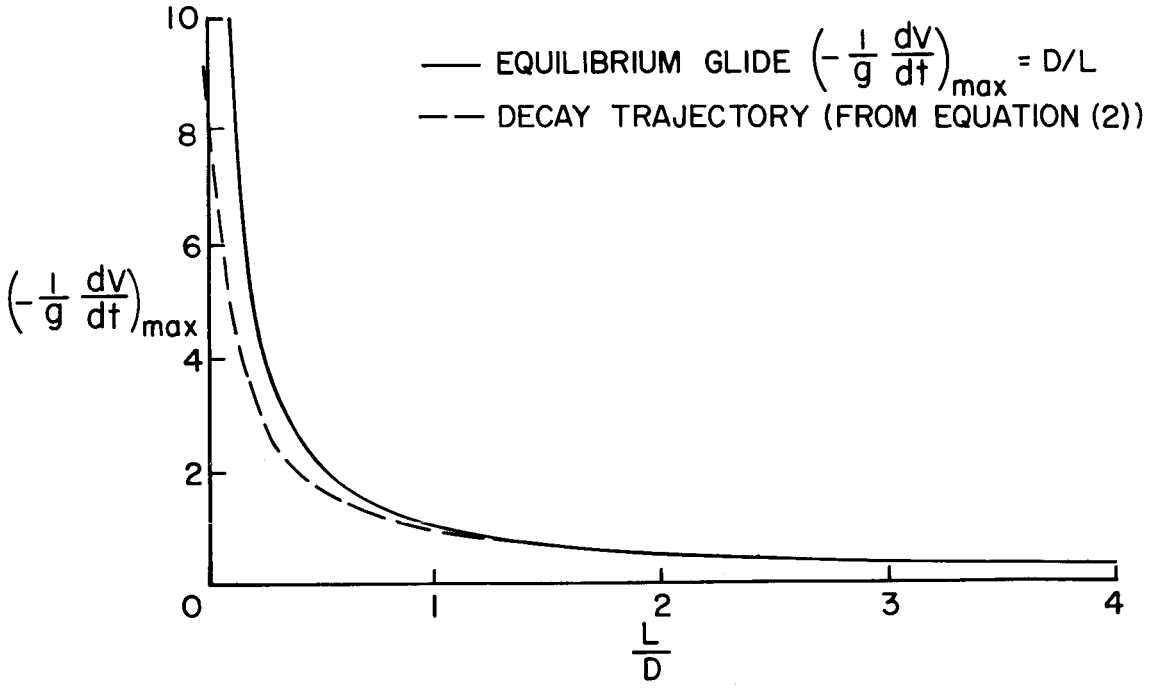

Figure 8.- Effect of lift-drag ratio on maximum deceleration of glide vehicles.

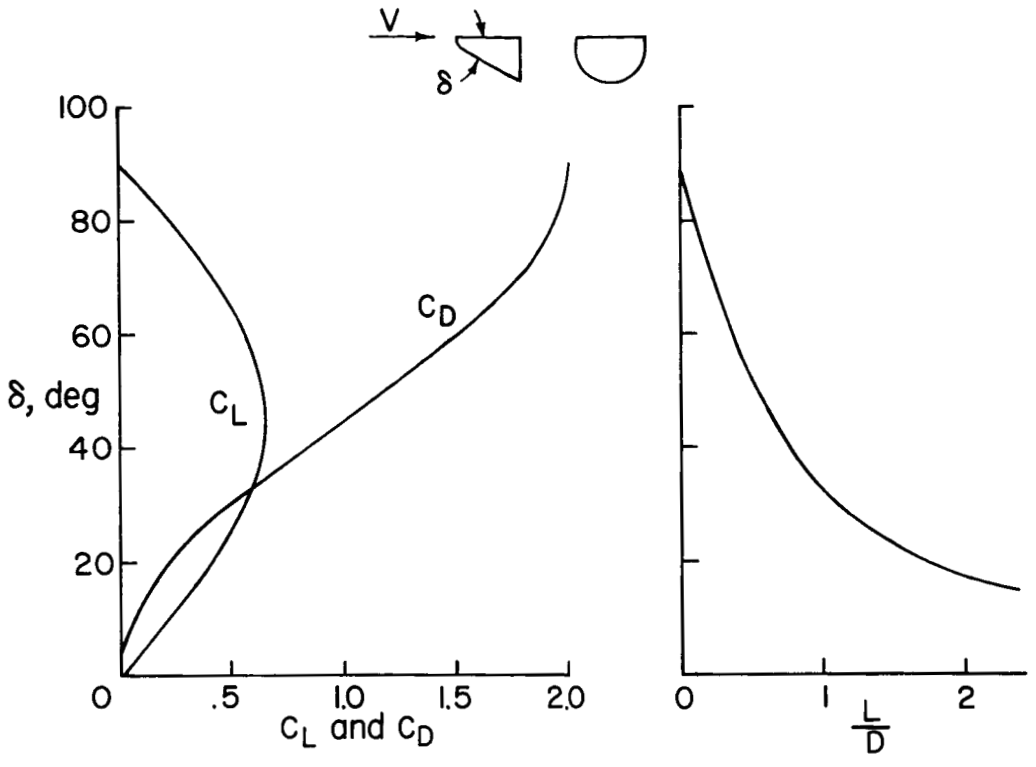

Figure 9.- Lift and drag of half-cones.

$A = 25\ ft^2$

$\sigma = 1\ ft$

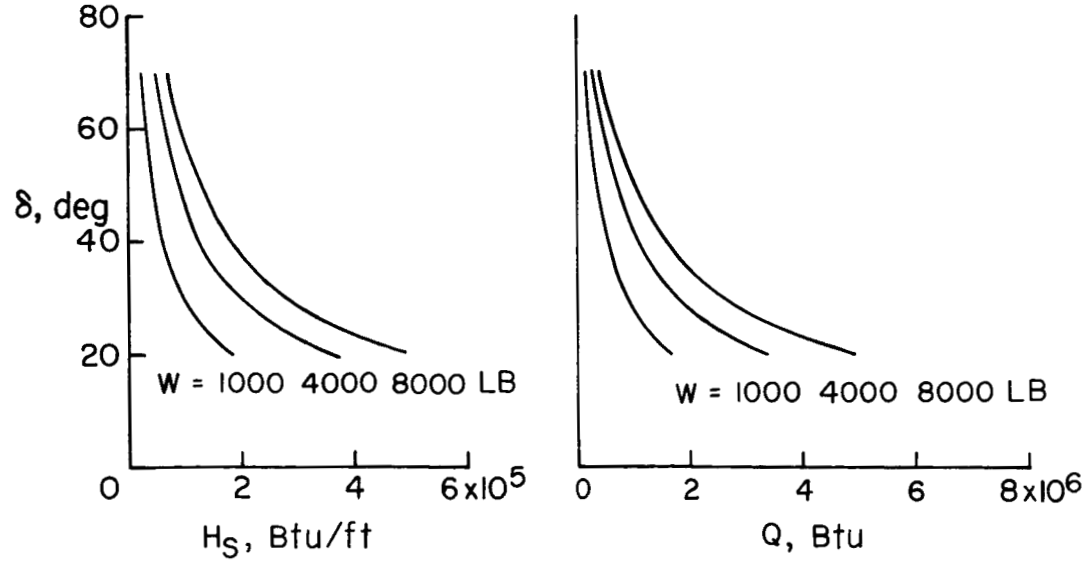

Figure 10.- Heating of conical glide vehicles during re-entry.

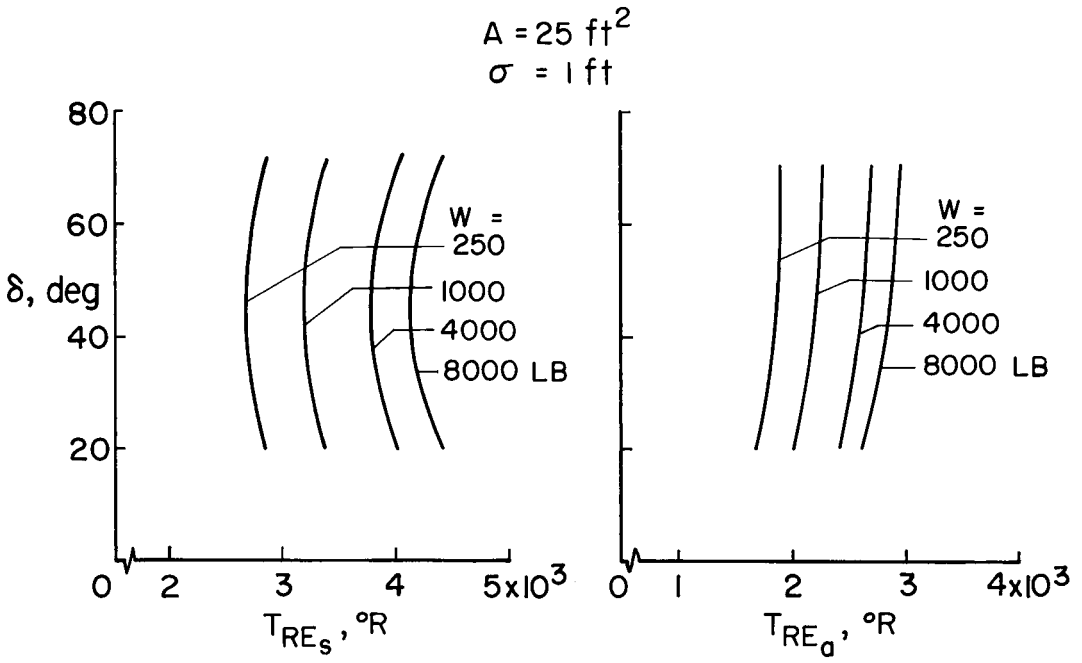

Figure 11.- Maximum radiation equilibrium temperatures of conical glide vehicles.

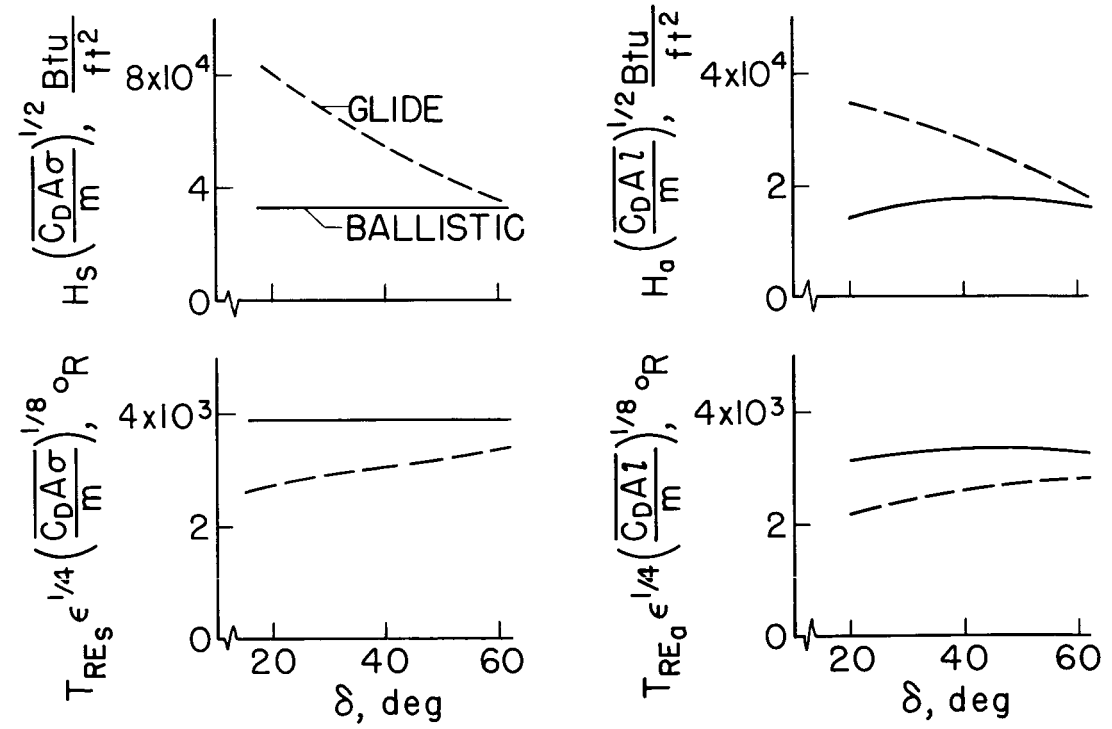

Figure 12.- Comparative heating of conical glide and ballistic vehicles ($\theta_E \rightarrow 0^\circ$).

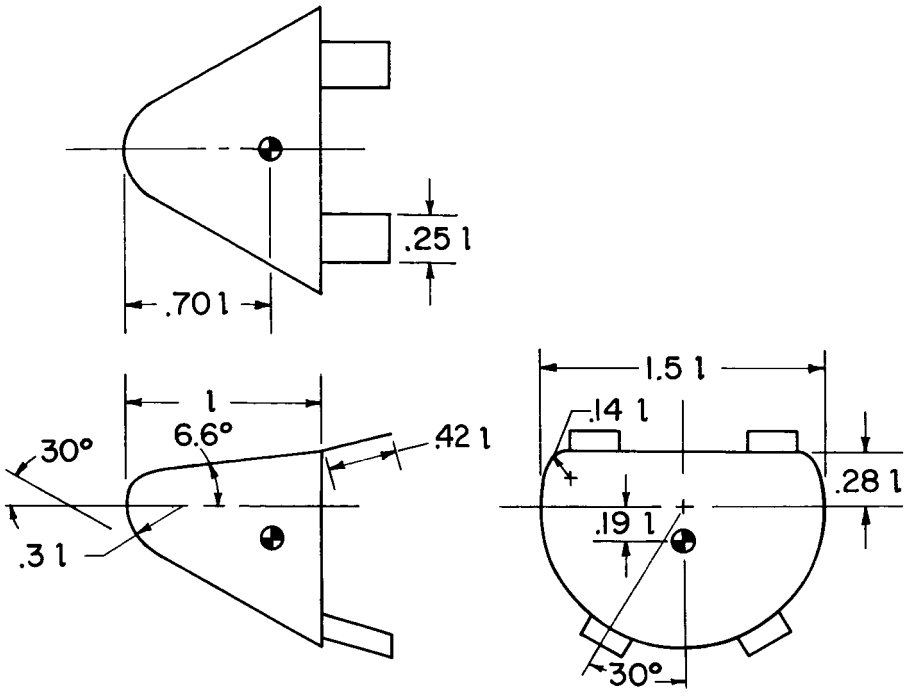

Figure 13.- Configuration studied.

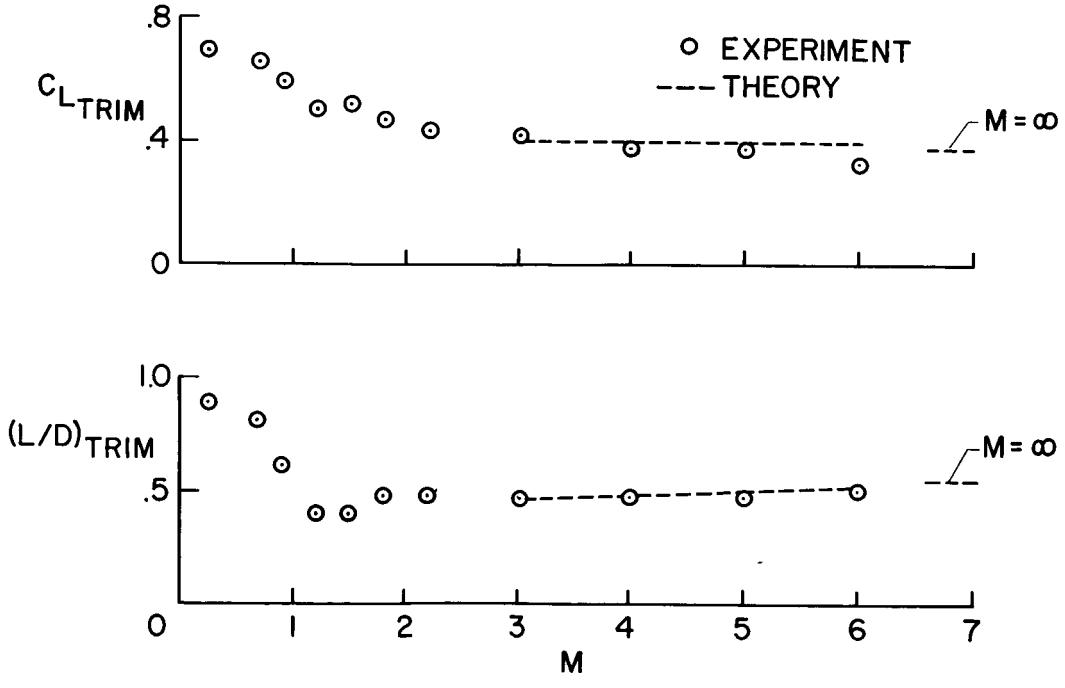

Figure 14.- Trimmed aerodynamic characteristics of study vehicle.

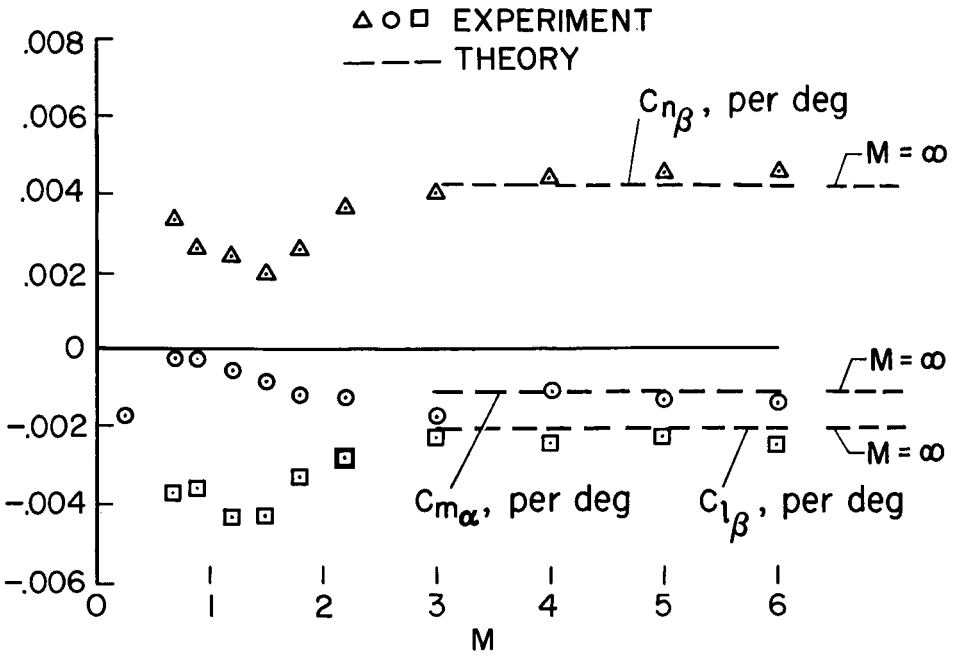

Figure 15.- Static stability of study vehicle.

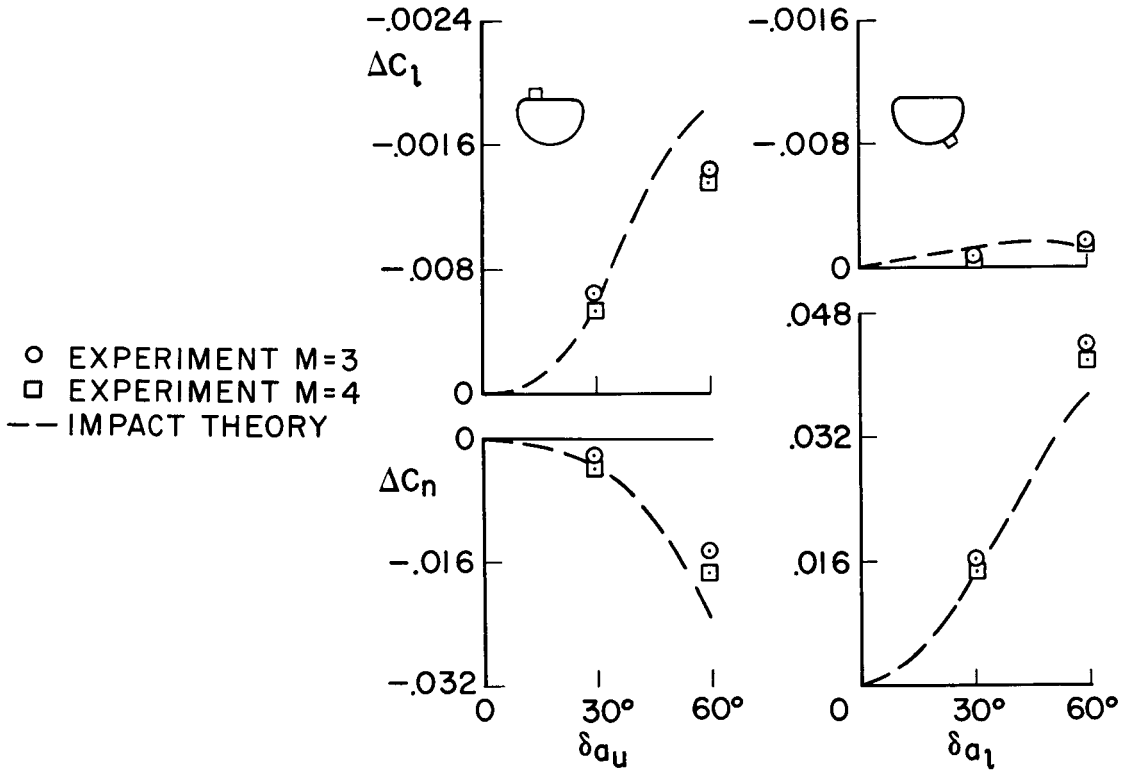

(a) Moments due to controls deflected as ailerons.

Figure 16.- Control characteristics.

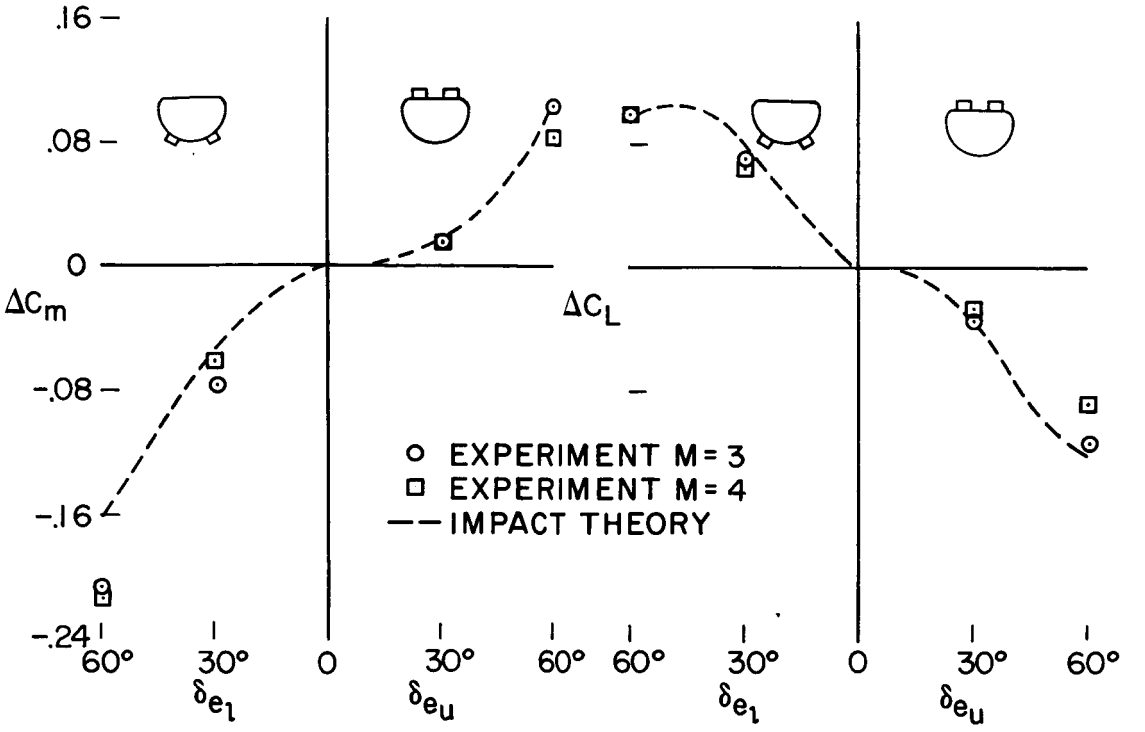

(b) Forces and moments due to controls deflected as elevators.

Figure 16.- Continued.

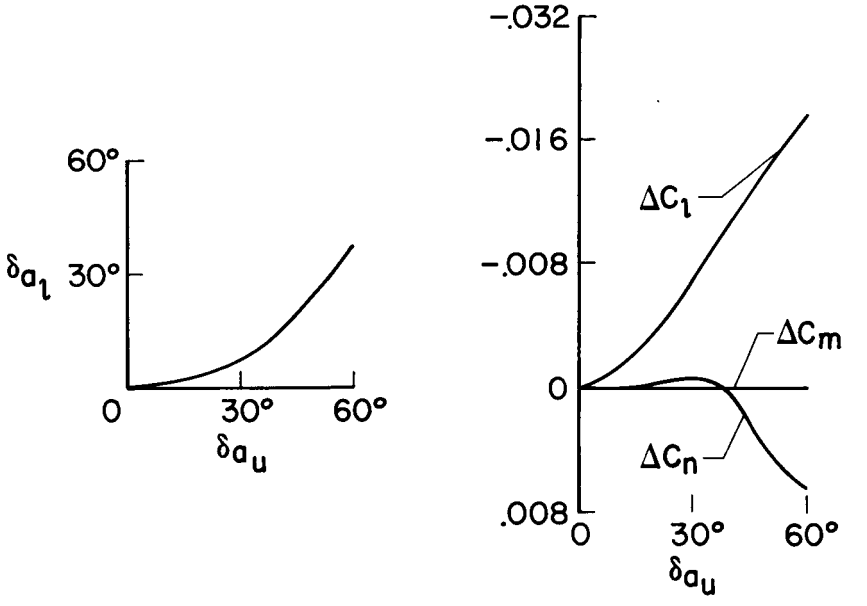

(c) Moments due to differentially deflected ailerons.

Figure 16.- Concluded.

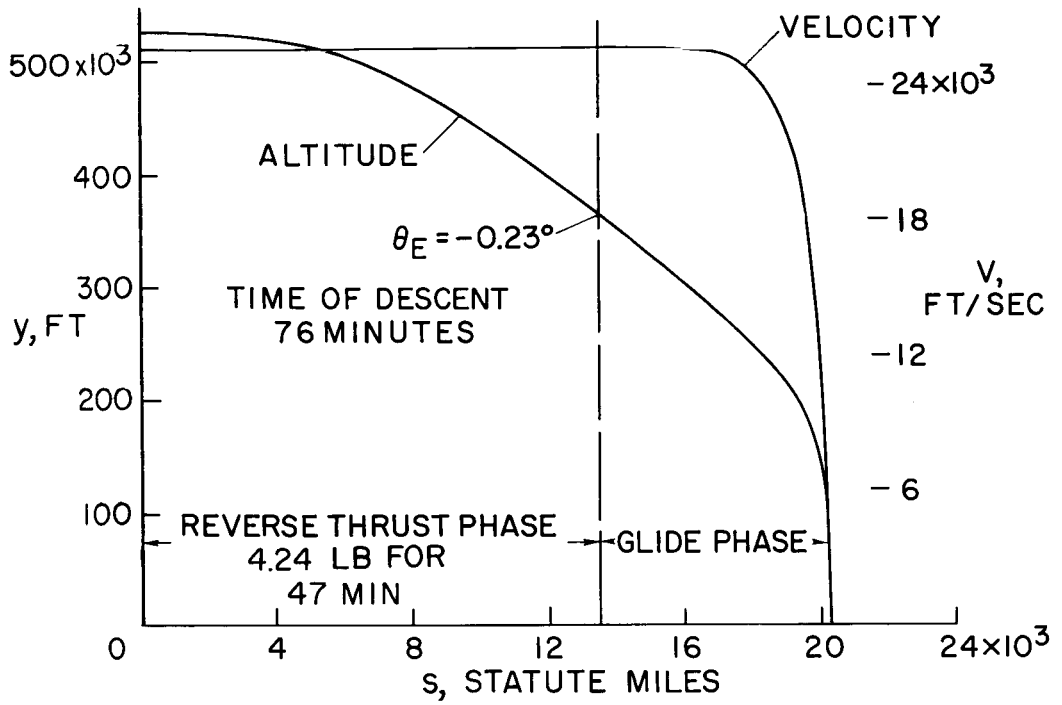

Figure 17.- Altitude and velocity variation during re-entry on an equilibrium glide trajectory.

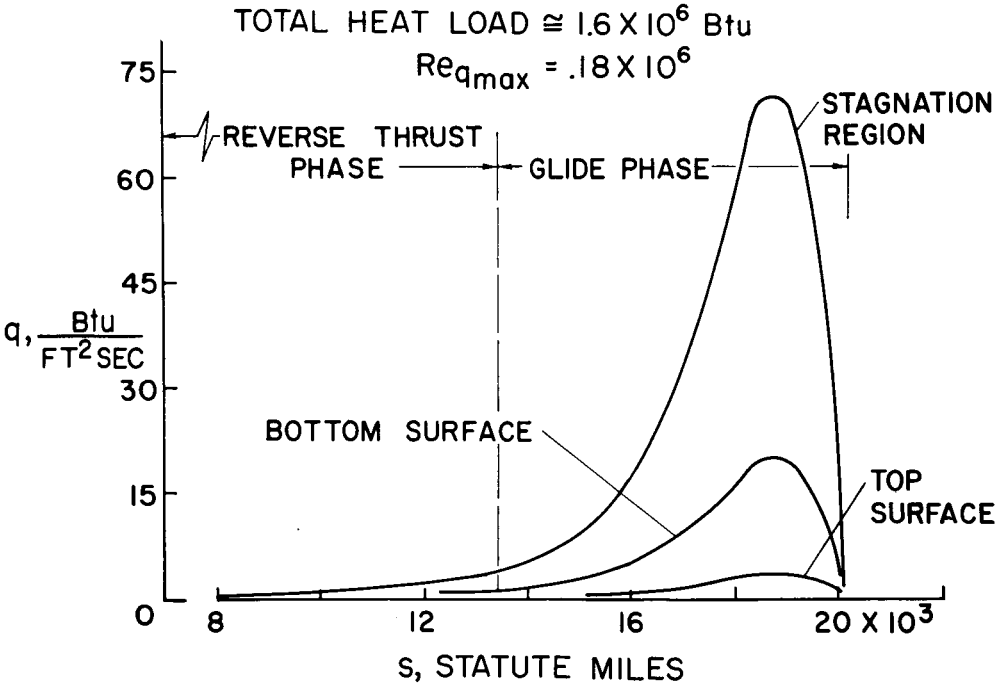

Figure 18.- Convective heating during re-entry on an equilibrium glide trajectory.

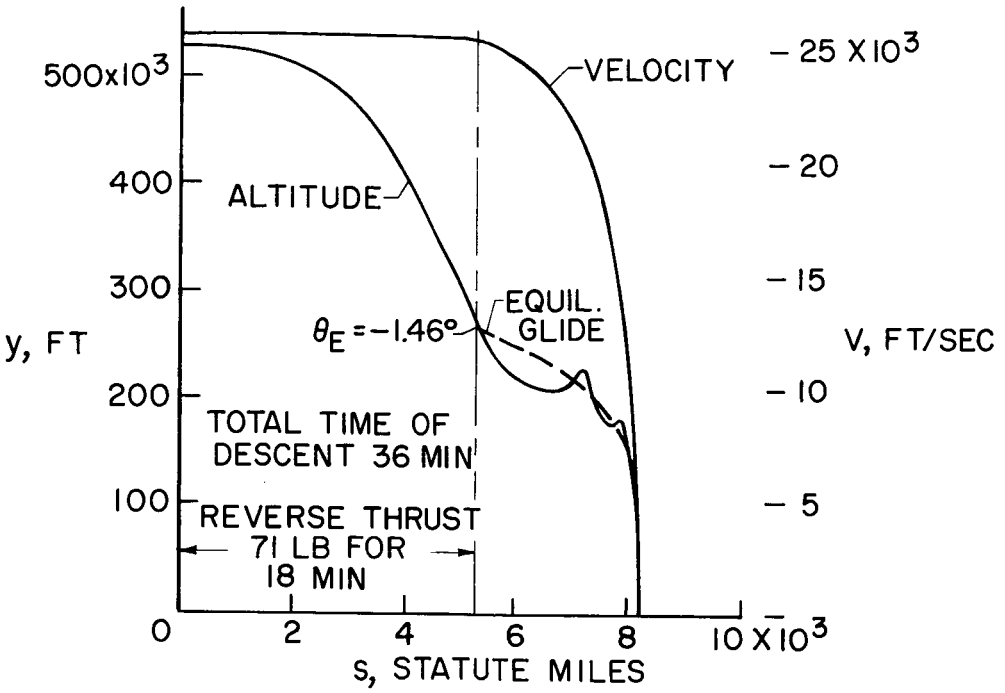

Figure 19.- Altitude and velocity variation during re-entry on an oscillatory trajectory.

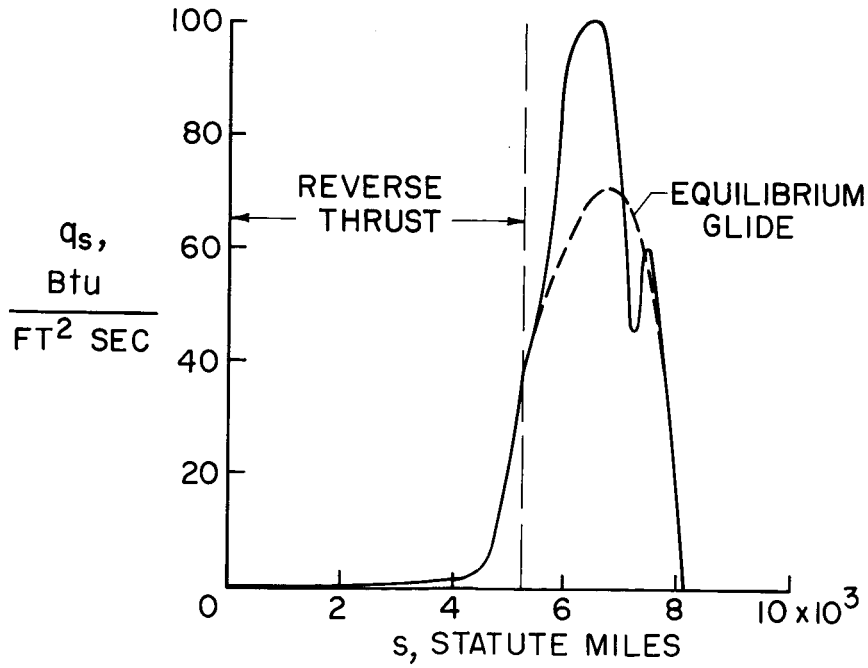

Figure 20.- Convective heating during re-entry on an oscillatory trajectory.

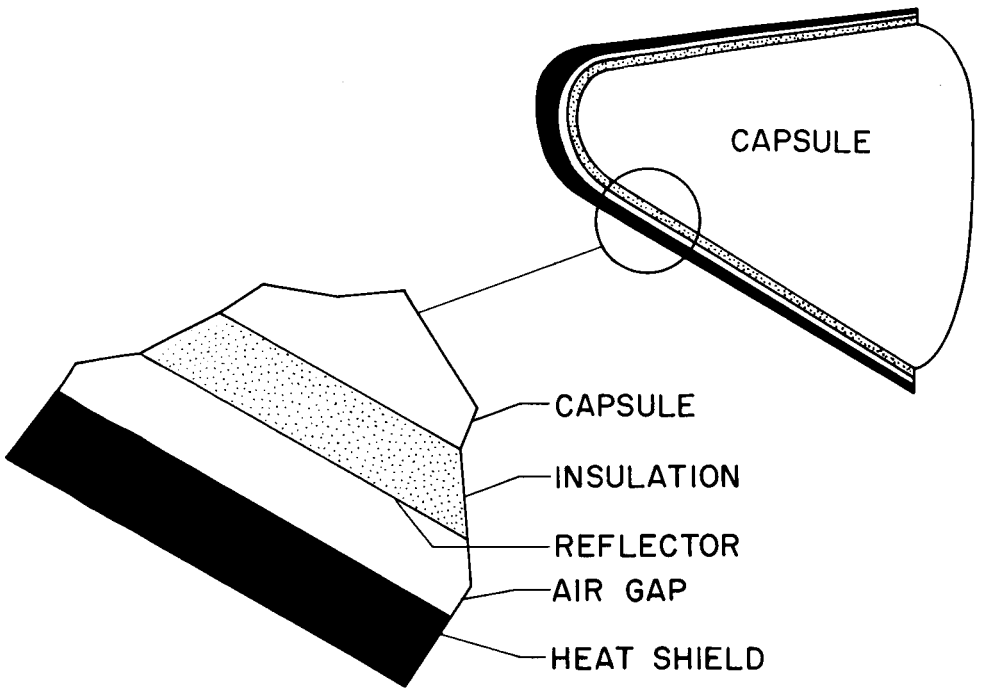

Figure 21.- Structure employed in study vehicle.

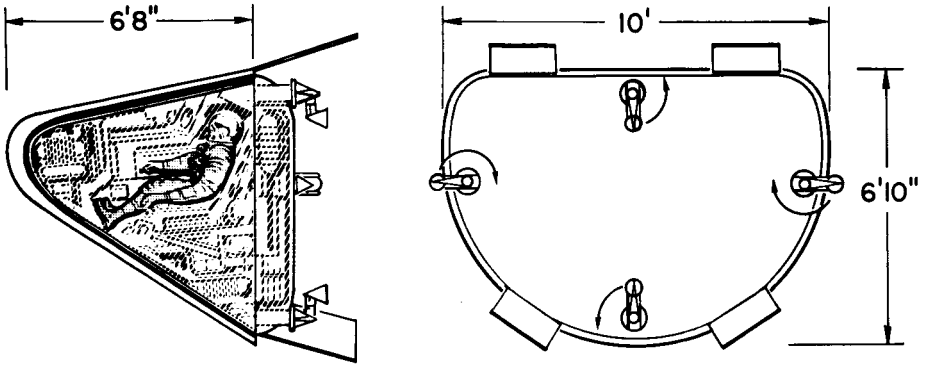

A. CAPSULE		2700 LB
1. Capsule Structure	400	
2. Pilot and Equipment	650	
3. Flight and Guidance Instruments	750	
4. Control and Recovery Equipment	700	
5. Research Instrumentation	200	
B. EXTERNAL STRUCTURE		1300 LB
TOTAL RE-ENTRY WEIGHT		4000 LB

Figure 22.- Study vehicle and weights.

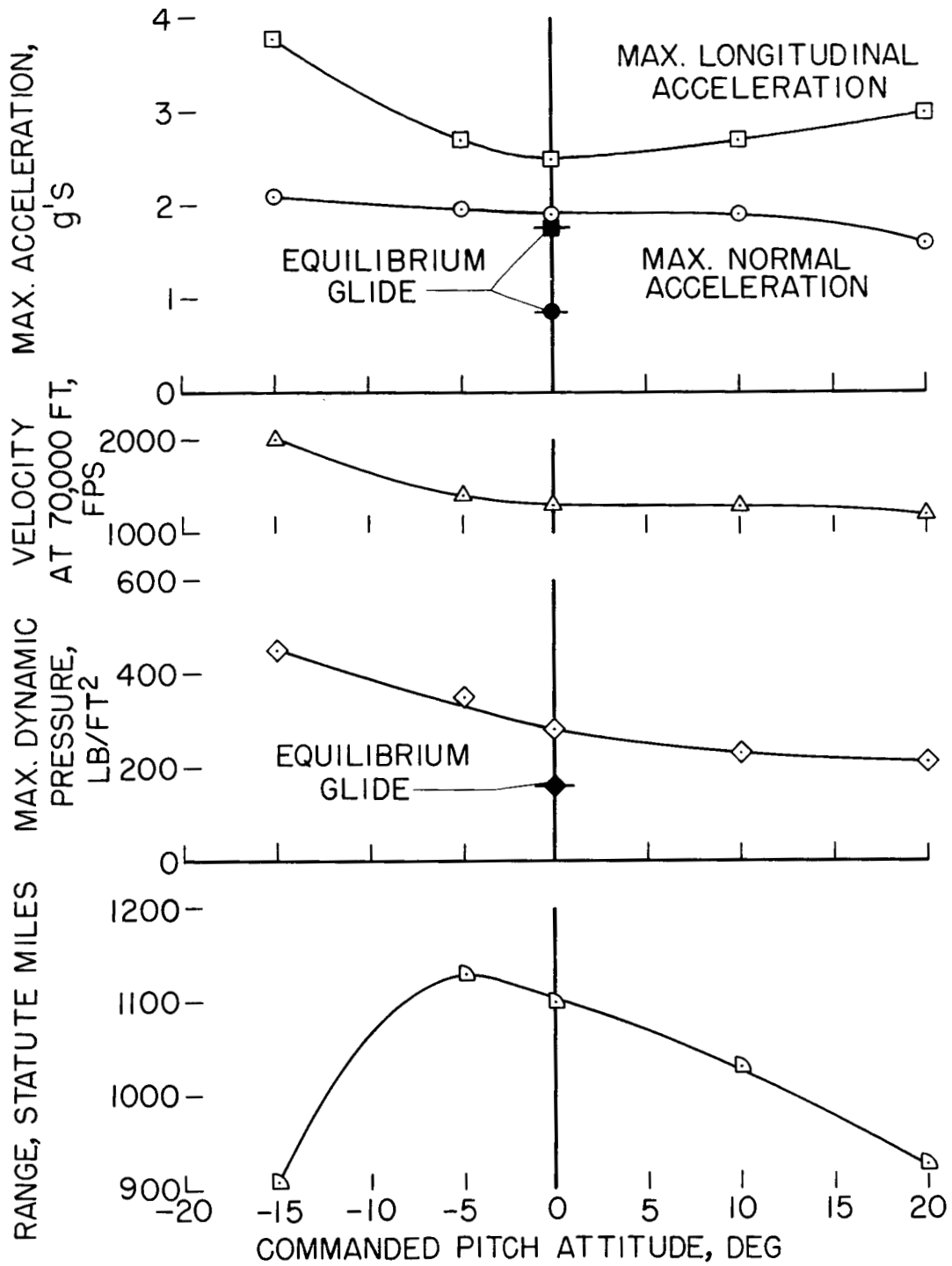

Figure 23.- Results of analog simulation of re-entry flight for various values of commanded pitch attitude down to 60,000 feet altitude (V_i = 22,000 feet per second, y_i = 270,000 feet).

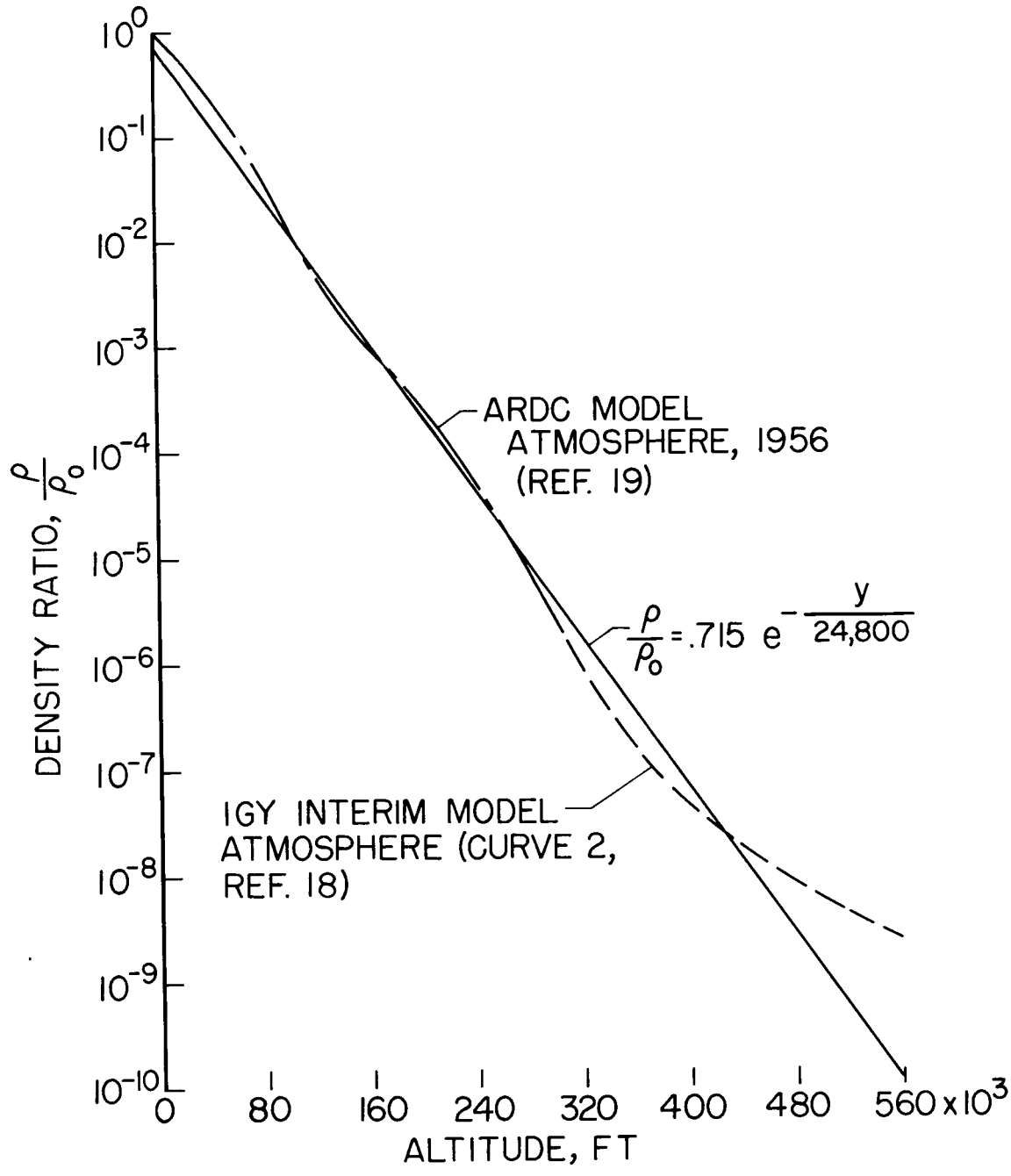

Figure 24.- Comparison of density ratios from the ARDC and IGY interim model atmospheres and exponential atmosphere.